




Schizophrenia-Linked Protein tSNARE1 Regulates Endosomal Trafficking in Cortical Neurons

Melissa Plooster,¹ Guendalina Rossi,¹ Martilias S. Farrell,²  Jessica C. McAfee,^{2,3} Jessica L. Bell,^{2,3} Michael Ye,¹  Graham H. Diering,^{1,3,5} Hyejung Won,^{2,3} Stephanie L. Gupton,^{1,3,4} and  Patrick Brennwald¹

¹Department of Cell Biology and Physiology, University of North Carolina, Chapel Hill, North Carolina 27599, ²Department of Genetics, University of North Carolina, Chapel Hill, North Carolina 27599, ³UNC Neuroscience Center, University of North Carolina, Chapel Hill, North Carolina 27599, ⁴Lineberger Cancer Center, University of North Carolina, Chapel Hill, North Carolina 27599, and ⁵Carolina Institute for Developmental Disabilities, University of North Carolina, Chapel Hill, North Carolina 27599

TSNARE1, which encodes the protein tSNARE1, is a high-confidence gene candidate for schizophrenia risk, but nothing is known about its cellular or physiological function. We identified the major gene products of *TSNARE1* and their cytoplasmic localization and function in endosomal trafficking in cortical neurons. We validated three primary isoforms of *TSNARE1* expressed in human brain, all of which encode a syntaxin-like Qa SNARE domain. RNA-sequencing data from adult and fetal human brain suggested that the majority of tSNARE1 lacks a transmembrane domain that is thought to be necessary for membrane fusion. Biochemical data demonstrate that tSNARE1 can compete with Stx12 for incorporation into an endosomal SNARE complex, supporting its possible role as an inhibitory SNARE. Live-cell imaging in cortical neurons from mice of both sexes demonstrated that brain tSNARE1 isoforms localized to the endosomal network. The most abundant brain isoform, tSNARE1c, localized most frequently to Rab7⁺ late endosomes, and endogenous tSNARE1 displayed a similar localization in human neural progenitor cells and neuroblastoma cells. In mature rat neurons from both sexes, tSNARE1 localized to the dendritic shaft and dendritic spines, supporting a role for tSNARE1 at the postsynapse. Expression of either tSNARE1b or tSNARE1c, which differ only in their inclusion or exclusion of an Myb-like domain, delayed the trafficking of the dendritic endosomal cargo Nsg1 into late endosomal and lysosomal compartments. These data suggest that tSNARE1 regulates endosomal trafficking in cortical neurons, likely by negatively regulating early endosomal to late endosomal trafficking.

Key words: endocytosis; GWAS; late endosome; schizophrenia; SNARE

Significance Statement

Schizophrenia is a severe and polygenic neuropsychiatric disorder. Understanding the functions of high-confidence candidate genes is critical toward understanding how their dysfunction contributes to schizophrenia pathogenesis. *TSNARE1* is one of the high-confidence candidate genes for schizophrenia risk, yet nothing was known about its cellular or physiological function. Here we describe the major isoforms of *TSNARE1* and their cytoplasmic localization and function in the endosomal network in cortical neurons. Our results are consistent with the hypothesis that the majority of brain tSNARE1 acts as a negative regulator to endolysosomal trafficking.

Received Mar. 16, 2021; revised Oct. 4, 2021; accepted Oct. 4, 2021.

Author contributions: M.P., G.R., J.C.M., J.L.B., M.Y., H.W., S.L.G., and P.B. designed research; M.P., G.R., J.C.M., J.L.B., M.Y., H.W., S.L.G., and P.B. performed research; M.P., G.R., J.C.M., J.L.B., M.Y., H.W., S.L.G., and P.B. analyzed data; M.P. and G.R. wrote the first draft of the paper; M.P., G.R., M.S.F., J.C.M., J.L.B., M.Y., H.W., S.L.G., and P.B. edited the paper; M.P., G.R., and P.B. wrote the paper; M.S.F., J.L.B., G.H.D., and H.W. contributed unpublished reagents/analytic tools.

This work was supported by National Institutes of Health Grants R01GM054712-23 to P.B., R01NS105614 and R35GM135160 to S.L.G., R00MH113823 and DP2MH122403 to H.W., K01MH108894 to M.S.F., and F31MH116576 and T32GM119999 to M.P. The datasets generated during and/or analyzed during the current study are available from the corresponding authors on reasonable request. We thank Dr. Patrick Sullivan for contributions during the early phases of this work; PsychENCODE, Dr. Jason Stein, Dr. Dan Liang (Stein laboratory), Mike Lafferty (Stein laboratory), and Dr. Joel Parker (Lineberger Bioinformatics Core) for assistance in quantifying RNA-sequencing data; Dr. Daniel Schrider for advice on comparing the conservation of tSNARE1 domains; Robert Currin and the Hooker Imaging Core at University of North Carolina for technical

assistance with microscopy; and the Exome Aggregation Consortium and the groups that provided exome variant data for comparison. The full list of contributing groups can be found at <https://gnomad.broadinstitute.org>. The Genotype-Tissue Expression Project was supported by the Common Fund of the Office of the Director of the National Institutes of Health; and by National Cancer Institute; National Human Genome Research Institute; National Heart, Lung, and Blood Institute; National Institute on Drug Abuse; National Institute of Mental Health; and National Institute of Neurological Disorders and Stroke. The data used for the analyses described in this manuscript were obtained from the Genotype-Tissue Expression Portal.

The authors declare no competing financial interests.

Correspondence should be addressed to Patrick Brennwald at pjbrennw@med.unc.edu or Stephanie L. Gupton at sgupton@unc.edu.

<https://doi.org/10.1523/JNEUROSCI.0556-21.2021>

Copyright © 2021 the authors

Introduction

Schizophrenia is a severe and heritable neuropsychiatric disorder. Common variation, copy number variation (CNV), and rare loss-of-function variation all contribute to its etiology. Genome-wide association studies (GWASs) have identified 145 loci associated with schizophrenia risk, but many of these loci are within noncoding regions, the functional impact of which is not well understood (Schizophrenia Working Group of the Psychiatric Genomics Consortium, 2014; Pardiñas et al., 2018). Functional genomic evidence, such as three-dimensional chromatin interactions and quantitative trait loci (QTL), successfully identified 321 high-confidence candidate genes for schizophrenia genome-wide significant (GWS) loci (Wang et al., 2018; Mah and Won, 2020). However, the causative role of these genes in schizophrenia pathogenesis remains to be studied; and for some, even the normal physiological function is not known. The next critical step is to study the function and dysfunction of these high-confidence candidates. *TSNARE1* is one of the high-confidence schizophrenia candidate genes (Wang et al., 2018), but its localization and function in the brain are presently unknown.

TSNARE1 arose from molecular domestication of a Harbinger transposon early in vertebrate evolution (Sinzelle et al., 2008; Smith et al., 2012). Harbinger transposons were an ancient transposon superfamily that encode a transposon protein and a SANT/Myb/trihelix DNA-binding protein. Active copies have not been identified in humans; however, some genes in the human genome trace their origin to Harbinger transposons (Kapitonov and Jurka, 2004). For example, *TSNARE1* and *NAIF* (nuclear apoptosis inducing factor) contain a domain descended from the DNA-binding protein encoding gene from Harbinger transposons (Sinzelle et al., 2008; Smith et al., 2012). *TSNARE1* encodes a fusion protein of this Myb-like tri-helix domain and a SNARE (soluble N-ethylmaleimide-sensitive attachment receptor) domain.

SNARE proteins are involved in the fusion of opposing lipid bilayers and are functionally conserved across all eukaryotes (Clary et al., 1990; Söllner et al., 1993; Rothman, 1994; Hanson et al., 1997; Lin and Scheller, 1997; Nichols et al., 1997). SNARE proteins promote membrane fusion by assembling into a four-helical SNARE complex. Distinct SNAREs in the complex impart specificity to the membranes that they fuse (Parlati et al., 2002). A highly conserved ionic layer within the hydrophobic center of the four-helical bundle of the SNARE complex is critical for SNARE complex assembly and subsequent membrane fusion (Antonin et al., 2002). The residue that the SNARE protein contributes to this ionic layer distinguishes SNARE proteins as either Q-SNAREs (glutamine) or R-SNAREs (arginine) (Fasshauer et al., 1998). A SNARE complex contains one R-SNARE and three Q-SNAREs, further classified as Qa, Qb, and Qc, based on sequence homology. A transmembrane (TM) domain or a membrane attachment site of the Qa SNARE is thought to be critical for allowing the free energy of the SNARE complex formation to be translated into membrane fusion (Hofmann et al., 2006).

Here we investigated the cellular function of tSNARE1. We validated three major gene products of *TSNARE1* in human brain. All isoforms contained a syntaxin-like Qa SNARE domain, and the majority lacked a TM domain as well as any other predicted site for membrane attachment. We defined the localization and function of tSNARE1 isoforms in the endolysosomal system of cortical neurons, which were consistent with a role for tSNARE1 in negatively regulating early endosome to late endosome membrane trafficking or maturation.

Materials and Methods

Animals. WT C57BL/6J background mice were purchased from The Jackson Laboratory and bred at the University of North Carolina at Chapel Hill (UNC). Mice are genotyped to confirm WT identity with standard genotyping procedures. Mice are kept in pathogen-free environments with 12 h light and dark cycles with ready access to food and water. Male and female mice were placed in a cage together overnight, and timed pregnant females were identified at E0.5 if the female had a vaginal plug. Sprague Dawley rats (G.H.D. laboratory, UNC) were acquired from Charles River Laboratory. All procedures and husbandry were conducted according to protocols approved by the Institutional Animal Care and Use Committee at UNC.

Plasmids. Stx6 human cDNA (BC009944), residues 1-255 in pGEX6P1 (pB2247). Stx12 human cDNA (BC046999), residues 1-278 in pGEX6P1 (pB2249). VAMP4 human cDNA (BC005974), residues 1-141 in pGEX6P1 (pB2258). Vit1a human cDNA (NM145206), residues 1-217 in pET15b (pB2246). Synthetic tSNARE1 (NP 001353833.1 codons optimized for *Escherichia coli* expression), residues 1-496 in pGEX4P1. tSNARE1a human cDNA (NM_145003.5) in pEGFP-C2 (pB2468). tSNARE1b human cDNA (NM_001291931.1) in pEGFP-C2 (pB2466). tSNARE1c human cDNA (NM_001366904.1) in pEGFP-C2 (pB2467). Stx12 human cDNA (BC046999) in pmCherry-C1 (pB2265). Human Rab7 in mTag-RFP-N1 (pB2357). Mouse Nsg1 in Halo-N1 (pB2504) was cloned from Nsg1-mCherry, a gift from B. Winckler (University of Virginia). TagRFP-Rab4a, TagRFP-Rab5a, and TagRFP-Rab11a were gifts from J.S. Bonifacino (National Institutes of Health). LAMP1-mCherry and Halo-N1 were a gift from J. Lippincott-Schwartz (HHMI Janelia). tagRFP-hRas-CAAX (tagRFP-CAAX) was a gift from R. Cheney (UNC). pCAG_Xph20-mRuby2-CCR5TC (PSD951B-mRuby2) was a gift from Matthieu Sainlos (Addgene plasmid #135531; <http://n2t.net/addgene:135531>; RRID: Addgene_135531) (Rimbault et al., 2021). All unique materials are readily available from the corresponding author on request.

Antibodies. Primary antibodies: anti-tSNARE1 was from LifeSpan Biosciences (catalog #LS-C160258) rabbit polyclonal Ab used at 1:1000 dilution for immunoblot analysis; another source for anti-tSNARE1 was from Sigma (catalog #SAB1303276) rabbit polyclonal Ab used at 1:25-1:120 dilution for immunofluorescence; anti-Stx6 was from Cell Signaling Technology (catalog #28 696) rabbit monoclonal Ab C34B2 used at 1:1000 dilution for immunoblot analysis; anti-Stx12 was from LifeSpan Biosciences (catalog #LS-B2989) mouse monoclonal Ab used at 1:1000 dilution for immunoblot analysis; anti-Vti1a was from LifeSpan Biosciences (catalog #LS-C160556) rabbit polyclonal Ab used at 1:1000 dilution for immunoblot; anti-Rab7 was from Sigma (catalog #R8779) mouse monoclonal Ab used at 1:50-1:100 dilution for immunofluorescence; anti-Tau was from Cell Signaling (catalog #4019) mouse monoclonal Ab used at 1:250 dilution for immunofluorescence; and anti-MAP2 was from Zymed (catalog #13-1500) mouse monoclonal Ab used at 1:100 dilution for immunofluorescence.

Secondary antibodies: AlexaFluor-488-conjugated AffiniPure Goat Anti-Rabbit IgG (H + L) was from Jackson ImmunoResearch Laboratories (catalog #111-545-144) used at 1:100 dilution for immunofluorescence; AlexaFluor-594-conjugated AffiniPure Goat Anti-Mouse IgG (H + L) was from Jackson ImmunoResearch Laboratories (catalog #115-585-146) used at 1:100 dilution for immunofluorescence.

***TSNARE1* mRNA identification.** Human Brain Total RNA (Takara, catalog #636530) and Human Brain Cerebral Cortex Total RNA (Takara, catalog #636561) were reverse-transcribed by Maxima H Minus First Strand cDNA Synthesis Kit (Thermo Fisher Scientific) with oligo (dT)₁₈ primers (1 μg RNA for each 20 μl reaction). The primers (Eurofins) used for *TSNARE1* transcript amplification are as follows: TSN1-NT3 (5'-gcatcaggatccaatcgccctggagggtggc-3'), TSN1-CT3 (5'-gcatcagctgatgatcaggggcagccacaagcagctgggggt-3'), and TSN1-CT2b (5'-gcatcagctgatgatccttcggcagaggtggcagatgatga-3'); 1 μl cDNA was amplified using 1 μl Phusion High-Fidelity DNA Polymerase (NEB) in HF Phusion buffer with 10 μM primers, 200 μM dNTPs (Agilent), ±5% DMSO per 50 μl reaction. Transcripts were checked on agarose gels, purified with phenol:chloroform:isoamyl alcohol and Wizard resin

(Promega), digested with XbaI and BamHI-HF in Cutsmart Buffer (NEB), and gel purified using Gel Extraction Kit (QIAGEN). Isolated transcripts were ligated into pEGFP-C2 using Quick Ligation Kit (NEB), cloned into DH5 α , purified with Wizard Genomic DNA Purification kit (Promega), and confirmed via Sanger sequencing (GeneWiz). The sequences of each of the four isoforms in this work can be found at NCBI: tSNARE1a (NM_145003.5 also known as variant 1), tSNARE1b (NM_001291931.1 also known as variant 2), and tSNARE1c (NM_001366904.1 also known as variant 7).

Transcriptomic data analysis. STAR-aligned bam files of adult PFC RNA-sequencing data were downloaded from PsychENCODE (Wang et al., 2018) and visualized with Integrative Genomics Viewer (Broad Institute). Sashimi plots were modified from Integrative Genomics Viewer to display exon coverage and the number of reads connecting the specific exons listed. Fetal cortical wall bam files were generously supplied from Jason Stein (de la Torre-Ubieta et al., 2018) (UNC) and analyzed as above. To determine the expression of *TSNARE1* in different brain regions, RNA-sequencing data were downloaded from Genotype-Tissue Expression (GTEx) (see acknowledgments) or the Allen Brain Atlas. To determine the expression of *TSNARE1* in different cell types, we used single-cell transcriptomic data from the adult brain (Darmanis et al., 2015; Lake et al., 2016).

Protein purification and SNARE assembly. Recombinant human Syntaxin6, Syntaxin12, and tSNARE1 were purified as previously described (Rossi et al., 1997), except that the GST-fusion proteins were cleaved with HRC 3C protease (Pierce) overnight at 4°C in buffer containing 50 mM Tris, pH 7.5, 150 mM NaCl, 1 mM EDTA, 0.5% Triton X-100, and 0.5 mM DTT. Recombinant human Vti1a was purified using His select nickel affinity column following the manufacturer's directions and dialyzed into buffer containing 20 mM Tris, pH 7.5, 150 mM NaCl, 10% glycerol, and 0.5% Triton X-100. Various combinations of soluble recombinant SNARE proteins (Syntaxin6, Vti1a, and Syntaxin12 or tSNARE1) were mixed with GST-Vamp4 immobilized on glutathione Sepharose beads in 100 μ l reactions with buffer containing 50 mM Tris, pH 7.5, 150 mM NaCl, 3 mM MgCl₂, 0.5% Triton X-100, and 0.5 mM DTT. All soluble proteins were present at 1 μ M final concentration while the GST-Vamp4 beads were present at 0.6 μ M final concentration. Soluble proteins were preincubated on ice for 20 min with Sepharose beads and then centrifuged at 13,000 rpm for 15 min at 4°C before adding to GST-Vamp4. The binding reaction was incubated overnight at 4°C, and the supernatants were then separated from the pellets by centrifugation. The pellets were washed 4 times in binding buffer and then boiled in SDS sample buffer for analysis by Coomassie and immunoblot. tSNARE1 inhibition assays were performed as described above, except that assays were incubated for 2 h at 4°C (rather than overnight) and concentrations of Stx12, Stx6, Vti1a, and GST-VAMP4 were adjusted to 0.4 μ M, while tSNARE1 concentrations varied from 0 to 6 μ M as depicted in Figure 5e–g.

For pulldown of heterologous SNARE complexes, mouse E15.5 embryo brains were dissected and lysed in 20 mM Tris, pH 7.5, 140 mM NaCl, 5 mM MgCl₂, 5% glycerol, and 0.5% Triton using a Dounce homogenizer. Lysate was left on ice for 20 min and then spun at 13,000 rpm at 4°C for 15 min. Lysate concentration was determined (Bradford, 1976), and adjusted to 25 mg/ml and before adding to immobilized beads of GST, GST-Vamp4, or GST-tSNARE1 at a final concentration of 1.5 μ M. Binding was conducted at 4°C for 2 h; and then the supernatant was separated from the beads, and the beads washed 4 times in binding buffer before boiling in sample buffer and analyzing by Western blot analysis.

Rodent neuron culture and transfection. For mouse cortical neurons, cortices were microdissected from both male and female E15.5 mouse embryos and either were plated immediately or stored in Hibernate E (Thermo Fisher Scientific) and plated within 24 h. Cortical neurons were dissociated with trypsin and plated on poly-D-lysine (Sigma)-coated imaging dishes (MatTek for endosomal colocalization, 8-well CellVis cover glass for Nsg1 trafficking), and grown and imaged in serum-free Neurobasal medium (Invitrogen) supplemented with 2% B27 (Invitrogen) and L-glutamine. For live-cell imaging of mouse cortical neurons at 2 DIV, neurons were centrifuged at 800 rpm for 7 min after

trypsinization, resuspended in transfection reagent (Amaxa Nucleofector; Lonza), and a nucleofector was used to electroporate the neurons according to the manufacturer protocol before plating on imaging dishes. To quantify colocalization of tSNARE1 with endosomal markers, 1 μ g of each GFP-tSNARE1 isoform was cotransfected into 2.5 million cells with 0.5–1 μ g of spectrally distinct red-tagged markers of the endosomal system (tagRFP-Rab4, tagRFP-Rab5, tagRFP-Rab11, tagRFP-Rab7, LAMP1-mCherry, and mCherry-Stx12). The Nsg1 trafficking experiments were performed by transfecting 2.5 million cells with 1 μ g Nsg1-HaloTag and 1 μ g of tagRFP-Rab4, tagRFP-Rab5, tagRFP-Rab7, tagRFP-Rab11, or LAMP1-mCherry, with or without 1 μ g GFP-tSNARE1. Directly before imaging, cells were incubated with 11.67 μ M AlexaFluor-660 HaloTag ligand (Promega) at 30°C for 5 min. The neurons were washed twice with fresh media and imaged.

Primary rat cortical neurons were prepared from both male and female E18 Sprague Dawley rats as previously described (Diering et al., 2014). Specifically, the cortex was microdissected, and the dissociated neurons were plated onto 8-well CellVis imaging dishes that had been pretreated with poly-L-lysine (Sigma Aldrich). Neurons were grown for the indicated days in glia-conditioned Neurobasal (Invitrogen) media supplemented with 2% B27, 1% horse serum, 2 mM GlutaMAX, and 100 U/ml penicillin/streptomycin (Invitrogen). For live-cell imaging, neurons were plated at 50,000–100,000 cells/well. Neurons were fed twice a week with fresh glia-conditioned media. For live cell-imaging, cortical neurons were transfected via Lipofectamine 2000 (Thermo Fisher Scientific) using a modified transfection protocol. The transfection conditions were as follows per well of a CellVis 8-well imaging dish: 0.25–1 μ g of GFP-tSNARE1c and 0.25–1 μ g tagRFP-Rab7, 0.25–1 μ g tagRFP-CAAX, or 0.25–1 μ g pCAG-Xph20-mRuby2-CCR5TC (PSD95IB-mRuby) was diluted in 25 μ l Neurobasal (Invitrogen). In a separate tube, 1.5 μ l Lipofectamine 2000 (Thermo Fisher Scientific) reagent was diluted in 25 μ l Neurobasal (Invitrogen). Each tube was mixed and incubated at room temperature for 5 min. The DNA-containing tube and Lipofectamine reagent-containing tube were mixed together and incubated at room temperature for 25 min. Half of the media from each well was removed and saved, and then the transfection solution was added dropwise to each well. The cells were placed in an incubator for 40 min. The transfection solution containing media was then aspirated from each well, and a mix of 50% old saved media and 50% fresh media was added to the well. Neurons were placed back in incubator until imaging.

Human cell culture and differentiation. SH-SY5Y cells were acquired from Sigma and maintained in media containing 45% F12 media (Invitrogen), 45% MEM (Invitrogen), and 10% FBS (Fisher). For immunofluorescence, SH-SY5Y cells were plated on poly-D-lysine (Sigma)-coated coverslips. Media was replaced with fresh media every 4–7 d. Primary human neural progenitor cells (NPCs) were plated at a density of 80,000 cells/well of a 12-well dish on nitric-acid washed 12 mm German Glass Cover Slips (Electron Microscopy Sciences) that were pretreated with poly-L-ornithine and laminin. NPCs were maintained in Neural Basal A (Invitrogen) supplemented with 100 μ g/ml Primocin (Invitrogen), 10% BIT 9500 (StemCell), 2 mM GlutaMAX (Invitrogen), 1 μ g/ml heparin, 40 ng/ml EGF/FGF, 4 ng/ml LIF, 20 ng/ml PDGF, and 10 ng/ml laminin. Cells were fed every 2–3 d by replacing half of the media with fresh media. To differentiate into human neurons, NPCs were plated on coverslips (80,000/well of a 12-well dish) and let grow for 3 d in the media described above. Cells were then differentiated by switching into Neural Basal A (Invitrogen) supplemented with 100 μ g/ml Primocin (Invitrogen), 2% B27 (Invitrogen), 2 mM GlutaMAX (Invitrogen), 10 ng/ml NT-3 (PeproTech), 10 ng/ml BDNF (PeproTech), and 5 ng/ml laminin. Half of the media was replaced with fresh differentiation media every 2–3 d until fixation at 14–15 DIV.

Immunofluorescence. At the indicated time points, cells were fixed in 4% PFA (Thermo Fisher Scientific Pierce) in PHEM fixative solution containing 60 mM PIPES, pH 7.0, 25 mM HEPES, pH 7.0, 10 mM EGTA, pH 8.0, 2 mM MgCl₂, and 0.12 M sucrose for 20 min in the dark at room temperature. Subsequent permeabilization and staining steps were performed in a humidified dark staining chamber at room temperature. Cells were either permeabilized in 0.5% SDS in 0.1 M HEPES-NaCl or 0.1% saponin (Sigma) in 1 \times PBS for 10 min. Cells were rinsed with 1 \times PBS and then blocked for 1 h in 5% normal goat serum (Jackson

ImmunoResearch Laboratories) in 1× PBS. Cells were rinsed with 1× PBS again and then incubated with the indicated primary antibodies in 1% normal goat serum and 0.1% Tween-20 in 1× PBS for 3 h. Cells were rinsed 3 times with 1× PBS for 5 min each. Secondary antibodies were incubated for 1 h in 1% normal goat serum and 0.1% Tween-20 in 1× PBS. Cells were rinsed 3 times with 1× PBS for 5 min each and then mounted onto slides with mounting media.

Microscopy. Pyramidal cortical neurons were imaged by confocal microscopy with an inverted 880 laser scanning microscope (Carl Zeiss) with a 32-channel GaAsP spectral detector and a Plan Apo 63× 1.4 NA oil objective (Carl Zeiss). For live-cell imaging, experiments were additionally performed in a humidified chamber at 37°C and 5% CO₂ when doing live-cell imaging. Simultaneous, bidirectional scans of *z* stacks with dual or triple channels, tight gate settings, and a 1-AU pinhole were acquired using the Carl Zeiss ZEN software. For Nsg1 trafficking assays, the chamber was set to 30°C and the pinhole was increased to maximize detection of endosomal surfaces. Movies of multiple neurons were recorded simultaneously, using the Positions function on the ZEN software and imaging once every 90 s for an hour.

Image analysis. For colocalization analysis, a *z* slice containing the majority of tSNARE1 puncta was chosen for quantification. Custom image-analysis software developed by the Taraska (Larson et al., 2014) laboratory was used to measure colocalization of puncta using MATLAB (The MathWorks). The program generates a ROI of 7 pixels radius around tSNARE1 (green) puncta and then uses the same ROIs in the marker (red) channel. It computes the colocalization in these ROIs based off two metrics, correlation (*C*), or the average Pearson's values of the ROIs, and peak height (*h*), which is the maximum intensity difference between the central pixel in the other (red) channel of the ROI and any other pixel in that ROI. Perfect colocalization would have a *C* and *h* value of 1.0, whereas perfect exclusion would have a *C* and *h* value of −1.0. To generate line scans, a 3 pixel-wide line was measured and averaged via ImageJ and graphed with Prism (GraphPad). For endogenous tSNARE1 localization, cells were picked that had nondiffuse cytoplasmic staining. tSNARE1 or Rab7 puncta were automatically detected with Imaris (Oxford Instruments) Surfaces function. Imaris's surface-surface colocalization MATLAB-based function was used to detect the percent of the volume that was colocalized. For Nsg1-HaloTag analysis, Imaris (Oxford Instruments) was used to quantify the percentage of Nsg1 puncta coincident with an endosomal marker over time. Movies were included if they were started by 9 min and 30 s after dye addition, did not bleach before the end of the movie, and had good signal:noise. For Nsg1, we automatically detected puncta over time using the Spots feature and manually removed points if picked up from fluorescence outside the cell. We used the Surfaces feature to automatically detect endosomal surfaces (tagRFP-Rab4, tagRFP-Rab5, tagRFP-Rab7, tagRFP-Rab11, or LAMP1-mCherry). We counted a Nsg1 puncta within an endosomal surface as long as its center point was within 0.03 μm from an endosomal surface. From this, we calculated the percentage of Nsg1 within an endosomal compartment for each time point. We rounded each time point to the nearest minute and a half increment to graph and analyze the data using GraphPad Prism.

Conservation analysis. We compared the phyloP scores between each domain, which measures nucleotide substitution rates that are more reduced (conservation) or increased (acceleration) than expected under neutral drift (Pollard et al., 2010). We compared the core SNARE domain (hg38 “-” strand, chromosome 8:142300633-142300647, chromosome 8:142284413-142284485, chromosome 8:142274781-142274851) with the Myb-like domain (hg38 “-” strand, chromosome 8:142344079-14234414). Because *TSNARE1* arose early in vertebrate evolution, we compared the phyloP scores for each of these domains using the 100 vertebrate pairwise alignment Conservation track from UCSC Genome Browser and reported as the mean ± SEM. Minor allele frequency was downloaded through the Ensembl genome browser, and the locations of the SNARE and Myb-like domain (above) were compared. CNV was reported using data from the Exome Aggregation Consortium (see acknowledgements) for each of the exons of *TSNARE1*. For the protein alignment between tSNARE1 and Stx12, we used DNASTAR.

Statistics and visualization. Multiple biological replicates were performed; and for imaging experiments, multiple neurons were imaged within each biological replicate. Graphs were generated with Microsoft Excel, Past4, or GraphPad Prism software and modified with Adobe Illustrator. ImageJ software (Schindelin et al., 2012, 2015; Schneider et al., 2012) (National Institutes of Health) was used for image visualization. Power analysis was performed for colocalization analysis using preliminary colocalization data. Experimental condition was blinded for analysis. For Nsg1 trafficking into Rab7⁺, Rab11⁺, or LAMP1⁺ compartments, the data were fit to a nonlinear regression one phase association model. For Nsg1 trafficking into Rab5⁺ or Rab4⁺ compartments, data were fit to a log-normal Gaussian distribution and were quantified by a one phase association, or a one phase decay model was separately fit to either the data before (*k*_{in}) or after (*k*_{out}) the maximum percentage of Nsg1 in Rab5⁺ compartments. The *k* and plateau values from these curve fits were plotted and compared. We assumed normal Gaussian distributions for all data unless otherwise noted. We compared groups using an ordinary one-way ANOVA with Dunnett's test for multiple comparisons against the control with 95% CIs. The exact *p* values are listed in the figure legends. For Nsg1 with Rab5, *F* (DFn, DFd) = 0.9 (2, 61) for *k*_{in} and *F* (DFn, DFd) = 0.9 (2, 62) for *k*_{out}. For Nsg1 with Rab7, *F* (DFn, DFd) = 11 (2, 49) for *k* and *F* (DFn, DFd) = 6.5 (2, 49) for plateau. For Nsg1 with LAMP1, *F* (DFn, DFd) = 5.7 (2, 59) for *k* and *F* (DFn, DFd) = 1.7 (2, 59) for plateau. For Nsg1 with Rab4, *F* (DFn, DFd) = 1.3 (2, 52) for *k*_{in} and *F* (DFn, DFd) = 0.2 (2, 55). For Nsg1 with Rab11, *F* (DFn, DFd) = 3.2 (2, 53) and *F* (DFn, DFd) = 0.3 (2, 53).

Results

TSNARE1 is a high-confidence candidate gene for schizophrenia risk

GWAS of schizophrenia identified 145 loci associated with schizophrenia risk (Pardiñas et al., 2018; Schizophrenia Working Group of the Psychiatric Genomics Consortium, 2014). One of the GWS loci mapped to an intronic region within the gene *TSNARE1*. The association of *TSNARE1* with schizophrenia was supported by multiple lines of functional genomic evidence, including expression QTLs (eQTLs) and three-dimensional chromatin interactions. For example, eQTLs of *TSNARE1* in the adult dorsolateral prefrontal cortex (DLPFC) colocalized with a schizophrenia GWAS locus in chromosome 8 (Fig. 1; posterior probability of colocalization = 0.97) (Wang et al., 2018). Transcriptome-wide association studies suggested overexpression of *TSNARE1* to be associated with schizophrenia (Bonferroni *p* = 3.65 × 10^{−7}), further confirming the colocalization results (Gandal et al., 2018). Isoform QTLs for *TSNARE1* were not associated with schizophrenia, which suggests that it is overexpression of every transcript of *TSNARE1* associated with schizophrenia rather than overexpression of a specific isoform. Hi-C results from the adult DLPFC revealed a physical interaction between the schizophrenia GWS SNPs and the promoter region of *TSNARE1*, which provides a potential mechanism by which schizophrenia-associated genetic risk factors are linked to *TSNARE1* regulation (Fig. 1) (Wang et al., 2018). Therefore, these results collectively suggest that *TSNARE1* is a significant and high-confidence candidate gene for schizophrenia risk. Yet, nothing is known regarding its cellular and physiological localization and function.

TSNARE1 gene expression is enriched in the cortex and in neurons

Because schizophrenia is a neuropsychiatric disorder, we wondered where within the human brain *TSNARE1* is enriched. RNA-sequencing data from the GTEx database suggested that *TSNARE1* expression was highest in the cortex as well as the cerebellum (Fig. 2*a*). We further examined fetal and adult human brain microarrays from the Allen Brain Atlas (Miller et al., 2014). Data from three microarray probes are available for

TSNARE1, but two of the three are within exon 14, an exon predicted to be alternatively spliced that would therefore not reflect expression of all isoforms. However, one probe (CUST_1054_P1416573500) maps to a region within exon 5, which is included in all predicted *TSNARE1* isoforms. This probe revealed enrichment of *TSNARE1* within regions of the cortex in both the fetal and adult human brain (Fig. 2*b*). We then leveraged single-cell RNA-sequencing results from the human cortex (Darmanis et al., 2015; Lake et al., 2016) to investigate cell type-specific expression profiles of *TSNARE1*. We found that *TSNARE1* was highly expressed in neurons and endothelial cells compared with other glial cell types (Fig. 2*c*). Specifically, *TSNARE1* was more enriched in excitatory neurons than in inhibitory neurons (Fig. 2*d*).

TSNARE1 is alternatively spliced, and the majority of transcripts lack a TM domain

Publicly available databases predicted a variety of *TSNARE1* isoforms (RefSeq), but which specific isoforms are expressed in the human brain were not known. The gene *TSNARE1* contains 15 exons (Fig. 3*a*). Exons 1 and 15 encode the 5' and 3' UTR, respectively. Predicted isoforms of *TSNARE1* contained a common N-terminal sequence encoded by exon 2 and one of two C-terminal exons: exon 14 that encodes a TM domain or exon 13 that encodes a non-TM domain. To identify the isoforms of *TSNARE1* expressed in human brain, we performed PCR using primer pairs against these regions with reverse-transcribed human adult cortical and total brain RNA. We validated three isoforms of *TSNARE1* in the human brain that differ in their C-termini and their inclusion or exclusion of exons 3 and 4 (Fig. 3*a*).

To determine the relative abundance of each of these isoforms in the human cortex, we data-mined RNA-sequencing data from the human adult DLPFC and human fetal cortical wall (Wang et al., 2018; de la Torre-Ubieta et al., 2018). We examined alternatively spliced regions using sashimi plots showing exon abundance and the number of reads overlapping two exons (Fig. 3*b,c*). Comparing the number of reads that link exon 2 to either exon 3 or exon 5, the majority of reads spliced exon 2 to exon 3 (Fig. 3*b*). In the other alternatively spliced region between exon 12 and exon 14, the majority of paired reads in exon 12 spliced to exon 13, and the abundance of reads in exon 14 was less than exon 13 (Fig. 3*c*). From these data, we

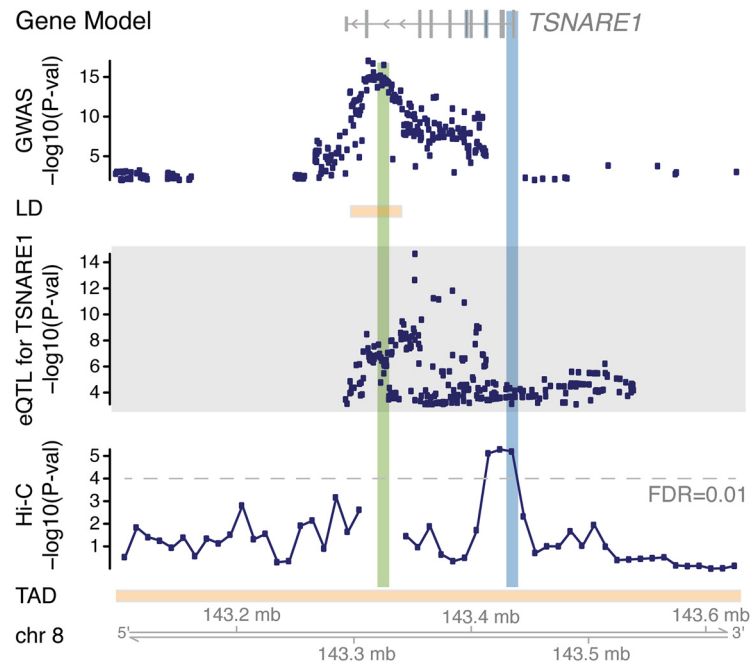


Figure 1. *TSNARE1* is a high-confidence candidate gene for schizophrenia risk. The association between *TSNARE1* and schizophrenia is supported by eQTL and Hi-C data. Hi-C $-\log_{10}$ (P-val) denotes the significance of interaction between schizophrenia GWS locus (highlighted in green) and each neighboring bin. Blue represents the *TSNARE1* promoter region. LD, Linkage disequilibrium; TAD, topologically associating domain.

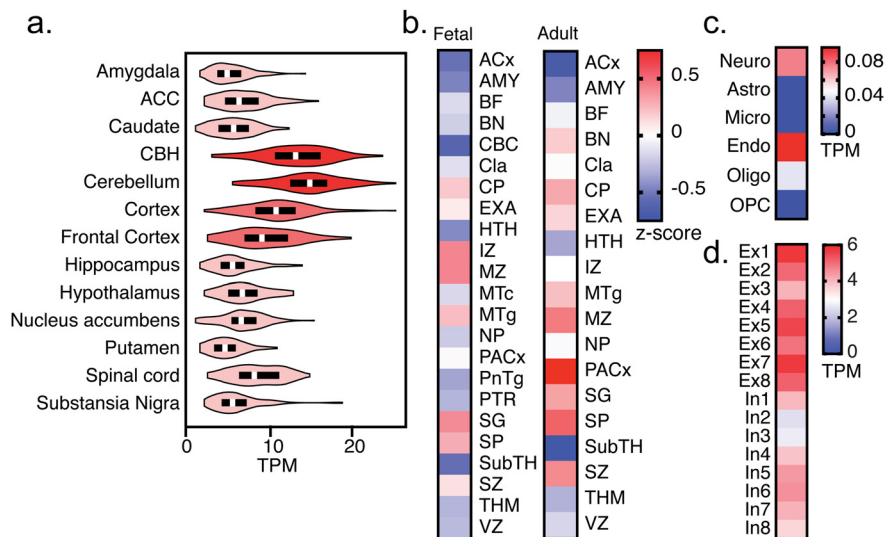


Figure 2. *TSNARE1* gene expression is enriched in the cortex and in neurons. *a*, GTEx brain RNA-seq data as plotted for transcripts per million bases (TPM) for *TSNARE1*. ACC, Anterior cingulate cortex; CBH, cerebellar hemisphere. *b*, Heat map of mean *TSNARE1* expression in brain structures in both the fetal (left) and adult (right) human brain. ACx, Allocortex; AMY, amygdaloid complex; BF, basal forebrain; BN, basal nuclei; CBC, cerebellar cortex; Cla, claustrum; CP, cortical plate; EXA, extended amygdala; HTH, hypothalamus; IZ, intermediate zone; MTc, midbrain tectum; MTg, midbrain tegmentum; MZ, marginal zone; NP, neural plate; PACx, periallocortex; PnTg, pontine tegmentum; PTR, pretectal region; SG, subplate granular zone; SP, subplate zone; SubTH, subthalamus; SZ, subventricular zone; THM, thalamus; VZ, ventricular zone. *c*, Heat map of mean *TSNARE1* expression in cell types in the brain. Astro, Astrocytes; endo, endothelial cells; micro, microglia; neuro, neurons; oligo, oligodendrocytes; OPC, oligodendrocyte progenitor cells. *d*, Heat map of *TSNARE1* expression in excitatory and inhibitory neurons. Ex, Excitatory neurons; In, inhibitory neurons.

imputed the approximate percentages of each isoform (Fig. 3*d*). The most abundant isoform was *tSNARE1c*, which includes exons 3, 4, and 13 (~80%–81%) (Fig. 3*d*). These data suggested that the majority of *TSNARE1* mRNA in the adult (~97%) and fetal (~93%) cortex includes the exon encoding a non-TM C-terminal

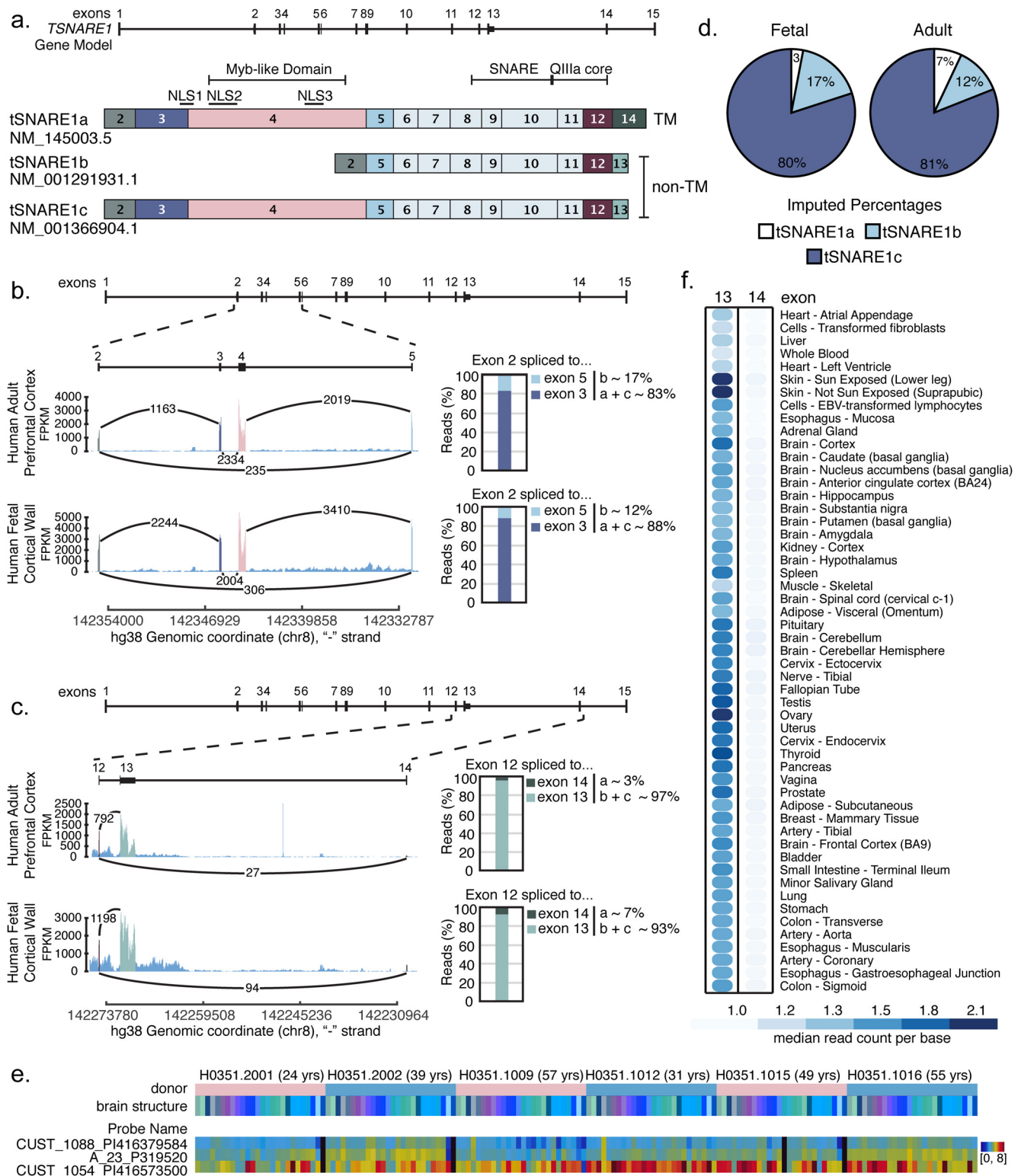


Figure 3. *TSNARE1* is alternatively spliced, and the majority of transcripts encode a C-terminal non-TM domain. **a**, The gene model for *TSNARE1* and the validated transcripts in adult human brain shown with exon inclusion and the predicted domains and nuclear localization signals (NLS) annotated above. **b**, **c**, Sashimi plot of RNA-sequencing data displaying exon coverage and the number of reads that link two exons from (**b**) exon 2 to either exon 3 or exon 5 or (**c**) exon 12 to exon 13 or exon 14. **d**, The imputed approximate percentages for each isoform calculated by combining the percentages determined in **b** and **c**. **e**, Heat map of the log₂ intensity of the probe common to all *TSNARE1* isoforms (CUST_1054_P1416573500) and those probes that are contained within exon 14 (CUST_1088_P1416379584, A_23_P319520). **f**, Heat map of the median read count per base for exons 13 and 14 from data adapted from GTEx.

domain. In agreement, the Allen Brain Atlas microarray data demonstrated that the probe common to all isoforms (CUST_1054_P1416573500) had higher expression than either of the two probes that map to the sequence encoding the TM domain in adult brain

tissues (Fig. 3e). This finding was not limited to the brain. RNA-sequencing data from GTEx revealed that, for every tissue, the non-TM domain encoded by exon 13 had higher expression than the TM domain encoded by exon 14 (Fig. 3f) (van de Leemput et al., 2014).

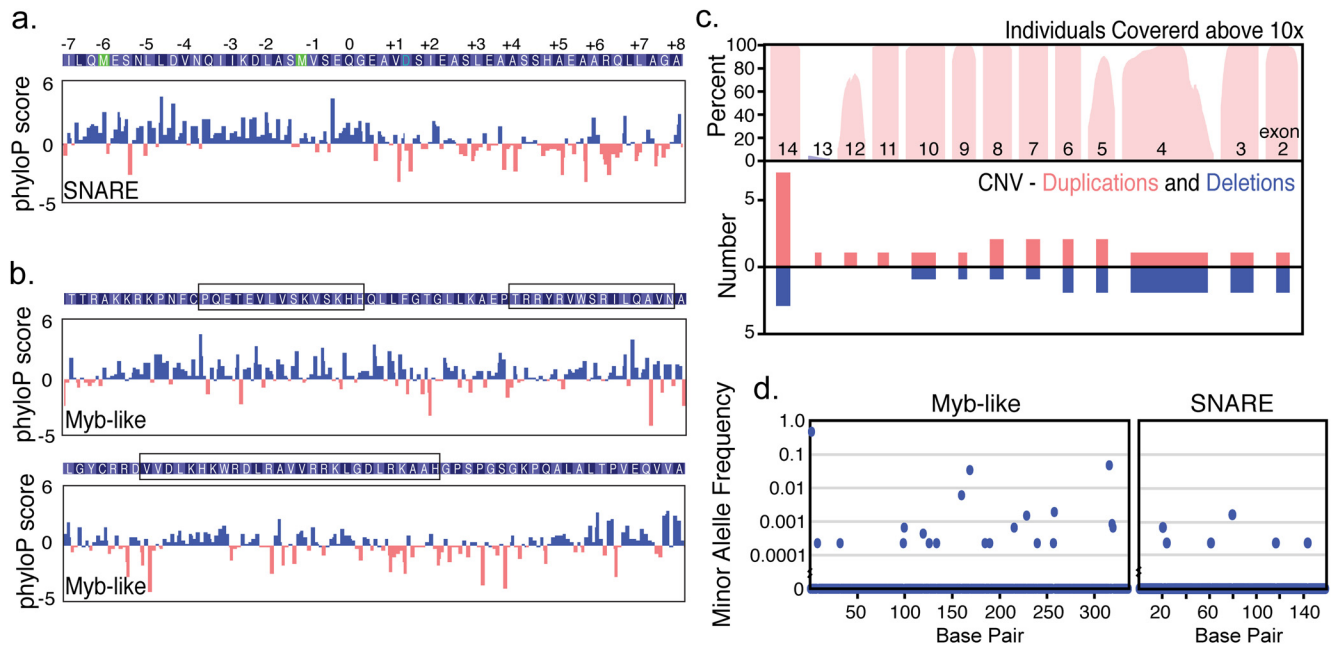


Figure 4. The SNARE and Myb-like domains of tSNARE1 are conserved. **a**, **b**, phyloP scores computed from 100 vertebrate alignment per base of the (**a**) SNARE domain with the layers of interacting amino acids within the four-helical bundle marked (mean = 0.4 ± 0.1 SEM) and (**b**) the Myb-like domain with the predicted three helices boxed (mean = 0.3 ± 0.1 SEM). Comparison of phyloP scores between Myb-like and SNARE domain determined by two-tailed Student's *t* test ($p = 0.374$). **c**, The percent of individuals with sequencing coverage above $10\times$ at each base (top) and CNV duplications and deletions (bottom) from the Exome Aggregation Consortium database. **d**, The minor allele frequency per base of each domain.

TSNARE1 encodes a SNARE and Myb-like domain

TSNARE1 encodes two predicted functional domains: an Myb-like domain and a SNARE domain (Fig. 3*a*). Isoforms that include exon four contain a predicted Myb-like domain, and all isoforms of tSNARE1 include a Qa SNARE domain encoded by exons 8–12 with the core of the SNARE domain encoded by exons 10–12. We wondered which domain might be more critical for tSNARE1 function. We expect a domain would be less tolerant of variation and have more sequence conservation if it is more critical to the function of tSNARE1. We found that both domains had a positive phyloP score, suggesting that both the SNARE domain (Fig. 4*a*) and the Myb-like domain (Fig. 4*b*) are evolutionarily conserved. A comparison of CNV (Fig. 4*c*) and minor allele frequency (Fig. 4*d*) between the SNARE domain and the Myb-like domain suggested that the SNARE domain may be under more evolutionary constraint, but the results were not significant. Since all the major products of *TSNARE1* contain the region encoding the SNARE domain, we proceeded to interrogate the role of this domain of tSNARE1 in further detail.

tSNARE1 is competent to form SNARE complexes with Stx6, Vti1a, and VAMP4

The observation that the majority of *TSNARE1* mRNA lacked a sequence to encode for a TM domain or any predicted site for membrane attachment is surprising. To our knowledge, tSNARE1 is the first Qa SNARE identified that lacks a TM domain or any site for membrane attachment. To confirm that tSNARE1 was competent to form SNARE complexes despite its unusual structure, we performed biochemical assays with endogenous and recombinant SNARE proteins *in vitro*. The SNARE domain of tSNARE1 shares its closest similarity with Syntaxin 12 (Stx12), a QaIII SNARE protein (Fig. 5*a*). Recombinant Stx12 forms a SNARE complex with recombinant endosomal SNARE proteins Stx6, Vti1a, and GST-VAMP4 (Zwilling et al., 2007). Recombinant tSNARE1c similarly formed a SNARE complex

with these recombinant endosomal SNARE proteins (Fig. 5*b*). Recombinant Stx12 potentiated the binding of recombinant Stx6 to GST-VAMP4 *in vitro* (Fig. 5*c*). Similarly, recombinant tSNARE1c potentiated this binding, although not to the degree of Stx12 (Fig. 5*c*). Finally, tSNARE1c-GST precipitated the endogenous SNARE protein Stx6 from embryonic murine whole-brain lysate (Fig. 5*d*). These data suggest that tSNARE1 was competent to form SNARE complexes with both recombinant and endogenous endosomal SNARE proteins *in vitro*.

Because tSNARE1 lacks a TM domain yet is capable of forming SNARE complexes, we hypothesized that tSNARE1 functions as an inhibitory SNARE (i-SNARE) (Varlamov et al., 2004). A defining feature of an i-SNARE is that it acts as a negative regulator of fusion by reducing the formation of fusion-competent SNARE complexes. It does this by generating fusion-incompetent SNARE complexes containing the i-SNARE in place of the functional SNARE. We performed an endosomal SNARE assembly assay to determine whether tSNARE1 inhibited the formation of SNARE complexes containing Stx12, Stx6, Vti1a, and VAMP4 (Fig. 5*e*). An increasing amount of recombinant tSNARE1c decreased Stx12 incorporation in SNARE complexes (Fig. 5*f*). These data demonstrated that tSNARE1 acts as a dose-dependent inhibitor with an IC_{50} of $2.0 \mu M$ (Fig. 5*g*) and therefore has the biochemical properties of an i-SNARE.

tSNARE1 localizes to markers of the endosomal network

Because we found that tSNARE1 is competent to form SNARE complexes *in vitro*, we wondered whether tSNARE1 would localize as expected for a membrane-associated protein, as discrete puncta in the cytoplasm. Considering that patients with schizophrenia present cortical abnormalities, excitatory pyramidal cortical neurons are implicated in schizophrenia, and *TSNARE1* is enriched in the cortex and in excitatory neurons (Fig. 2), we measured the localization of GFP-tSNARE1 specifically in murine pyramidal-shaped excitatory cortical neurons (Rimol et al.,

SNARE complexes *in vitro*, we hypothesized that tSNARE1 functions within the endolysosomal system. The endolysosomal system is responsible for sorting, recycling, and degradation of internalized cargo. Internalized cargo arrives at Rab5⁺ early endosomes and can be recycled back to the plasma membrane via two separate routes: Rab11⁺ recycling endosomes or Rab4⁺ rapid recycling compartments. Alternatively, cargo is sent from Rab5⁺ early endosomes to Rab7⁺ late endosomes and LAMP1⁺ lysosomes for degradation. To determine to which compartment tSNARE1 localizes, we cotransfected murine cortical neurons with GFP-tSNARE1 isoforms and spectrally distinct red-tagged markers of the endosomal network (Fig. 6a).

We noted that the majority of tSNARE1 signal localized to the perinuclear region of the soma. We quantified colocalization in the soma using a custom image analysis software that specifically measured colocalization of puncta, which represent membrane-bound organelles (Larson et al., 2014). Each isoform of tSNARE1 colocalized positively with a number of the endosomal markers, but the isoforms displayed unique localization patterns (Fig. 6b). tSNARE1b and tSNARE1c, which lack a TM domain, most frequently populated compartments of the late endosome marked by Rab7⁺ puncta (Fig. 6c). tSNARE1a, the TM domain containing isoform, colocalized markedly with Stx12 (Fig. 6c), which itself localized to multiple endosomal compartments. These data indicated that the most abundant isoforms of tSNARE1 in the brain localized to Rab7⁺ late endosomal compartments. To determine whether tSNARE1c also colocalized with Rab7 in more mature neurons, we turned to rat cortical neurons. Live-cell confocal microscopy of rat cortical neurons at 15 DIV demonstrated that GFP-tSNARE1c colocalized with tagRFP-Rab7 in more mature rat neurons (Fig. 6d,e), in agreement with the data from immature mouse neurons.

Endogenous tSNARE1 localizes to Rab7⁺ compartments

Because the previous data relied on exogenous expression of human tSNARE1 and endosomal markers in rodent neurons, which lack endogenous tSNARE1, we sought to determine whether endogenous tSNARE1 in human cells localized similarly. We performed immunofluorescence with antibodies against both human tSNARE1 and Rab7 on primary human NPCs. We used an antibody for tSNARE1 whose epitope is within the SNARE domain of tSNARE1 and should therefore recognize all isoforms of tSNARE1. Endogenous tSNARE1 localized as discrete puncta within the cytoplasm, and these discrete puncta were often coincident with Rab7 (Fig. 7a–c). Similar results were observed for endogenous tSNARE1 and Rab7 in the neuroblastoma cell line SH-SY5Y (Fig. 7d–f). These data suggest that tSNARE1 localizes to late endosomes in human cells, supporting our observations using exogenous GFP-tSNARE1 in rodent neurons.

Overexpression of tSNARE1 delays trafficking of Nsg1 into late endosomal and lysosomal compartments

Because tSNARE1 most frequently populated compartments of the late endosome, we hypothesized that tSNARE1 regulates trafficking at this compartment. *TSNARE1* is absent from several vertebrate genomes (Ensembl), including rodents, perhaps because of a transposition event early in these lineages (Sinzelle et al., 2008; Smith et al., 2012). We used the mouse to exogenously express GFP-tSNARE1 in neurons and compare with a “natural” KO to interrogate its effect on endosomal trafficking. To determine how tSNARE1 regulates trafficking through the endosomal system, we quantified how overexpression of tSNARE1

altered the trafficking of the dendritic endosomal cargo protein Nsg1/Neep21. Nsg1 is a Type II TM protein, which interacts with Stx12 and is rapidly endocytosed and trafficked from the early endosome to the late endosome and the lysosome where it is degraded (Steiner et al., 2002; Barford et al., 2017; Yap et al., 2017). We measured the localization of a transient population of Nsg1-HaloTag in murine cortical neurons at 2 DIV, marked by a pulse of a cell-impermeable fluorescent HaloTag ligand, as it trafficked through the endosomal network with or without GFP-tSNARE1 isoforms (Fig. 8a–c; Movies 1, 2, 3).

Nsg1 rapidly colocalized with Rab5⁺ compartments and slowly left over an hour time period. There was no difference between the rate of Nsg1 puncta entering or exiting Rab5⁺ early endosomes with or without expression of tSNARE1b or tSNARE1c (Fig. 8d,e). Strikingly, expression of either tSNARE1b or tSNARE1c delayed entry of Nsg1 into Rab7⁺ compartments, and Nsg1 never reached the extent of colocalization with Rab7 as it did in the absence of tSNARE1 (Fig. 8f,g). Overexpression of tSNARE1b or tSNARE1c also delayed entry of Nsg1 into LAMP1⁺-associated compartments (Fig. 8h,i). As the only difference between tSNARE1b and tSNARE1c is the exclusion or inclusion of the Myb-like domain, this finding suggested that the Myb-like domain does not regulate Nsg1 trafficking through the endosomal system. Therefore, the SNARE domain of tSNARE1 delayed trafficking of Nsg1 into Rab7⁺ late endosomal and LAMP1⁺ lysosomal compartments.

Nsg1 trafficking from the early endosome to the late endosome and lysosome is well characterized, but Nsg1 also colocalizes with Rab4⁺ endosomes, and, to a lesser extent, in Rab11⁺ endosomes (Steiner et al., 2002). To determine whether tSNARE1 expression affects the trafficking of Nsg1 to Rab4⁺ or Rab11⁺ recycling compartments, we performed our Nsg1 trafficking assay with these endosomal markers. In agreement with previous literature, we found that a population of Nsg1 trafficked into Rab4⁺ endosomal compartments, the recycling compartment most proximal to the early endosome (Fig. 8j). However, there was no significant difference between the rate of Nsg1 puncta entering or exiting Rab4⁺ rapid recycling compartments with or without expression of tSNARE1b or tSNARE1c (Fig. 8k). In contrast, very little Nsg1 entered the recycling compartment most distal to the early endosome, the slower Rab11⁺ recycling endosome (Fig. 8l). Expression of tSNARE1b or tSNARE1c did not affect Nsg1 trafficking to this compartment (Fig. 8m). These data demonstrate that tSNARE1 inhibits Nsg1 trafficking into Rab7⁺ late endosomes and LAMP1⁺ lysosomes but does not affect trafficking into Rab5⁺ early endosomes or Rab4⁺ or Rab11⁺ recycling compartments. These data suggest that tSNARE1 specifically regulates trafficking to the late endosome, likely by negatively regulating early endosome to late endosome trafficking or maturation.

tSNARE1 localizes to axons, dendrites, and the postsynapse

tSNARE1 is a schizophrenia-associated protein that localizes to and functions in the endosomal network. Yet, how dysfunction of tSNARE1 contributes to schizophrenia pathogenesis is unknown. A characteristic of schizophrenia is alterations in brain connectivity. To determine whether tSNARE1 was poised to contribute to changes in brain connectivity, we examined tSNARE1 compartmentalization in neurons. We generated human neurons differentiated from primary human NPCs and immunostained endogenous tSNARE1, which revealed that tSNARE1 was enriched in the soma and sometimes localized to the nucleus (Fig. 9a), similar to rodent neurons. Discrete tSNARE1 puncta were also observed in neuronal processes. NPC-derived human neurons costained for tSNARE1 and either Tau or MAP2

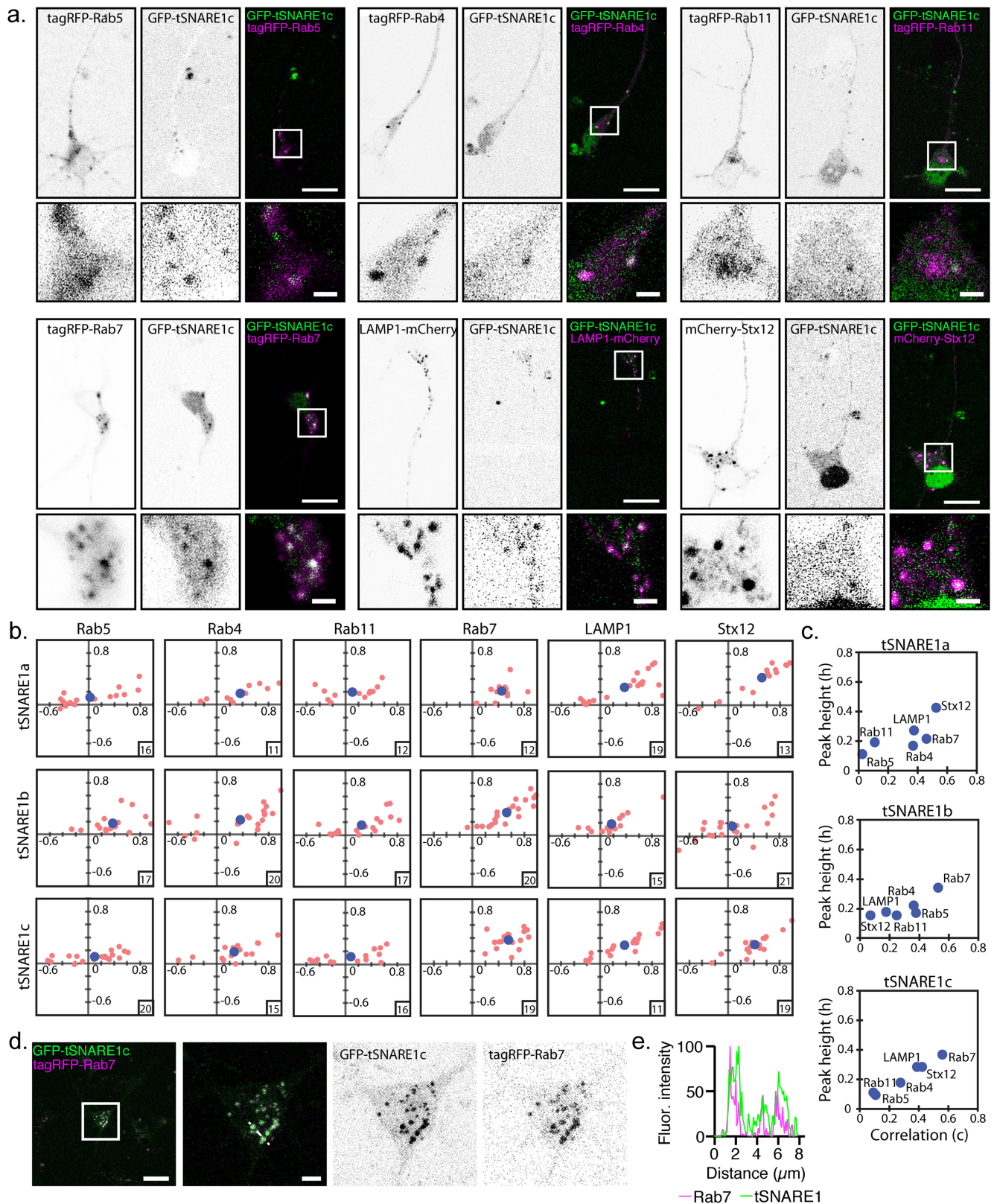


Figure 6. tSNARE1 localizes to markers of the endosomal network in cortical neurons. **a**, Example images of 2 DIV E15.5 murine cortical neurons expressing GFP-tSNARE1c and various red-tagged endosomal markers. For each group, reverse-contrast images of each channel are shown with a merged image to the right. A zoomed-in region of the soma marked by a white box in the merged image is shown below each group. Scale bars: 15 μm ; zoom, 2.5 μm . **b**, Quantification of colocalization using peak height and correlation of GFP-tSNARE1 isoforms with each marker. The number (*n*) of (cells) is boxed on each individual distribution. At least three independent biological replicates were performed for each condition. **c**, Averages of individual distributions for each isoform as shown in **b**. **d**, A maximum intensity projection of a 15 DIV E18 rat cortical neuron expressing GFP-tSNARE1c and tagRFP-Rab7, shown in a zoomed-out image (left) with a zoomed-in ROI (right). Beside this are inverted contrast images of each channel from the merged images. Scale bars: left, 25 μm ; zoomed images, 5 μm . **e**, Average 3 pixel-wide line scan of the fluorescence intensity of GFP-tSNARE1c and tagRFP-Rab7 in a single z plane (normalized to the minimum and maximum fluorescence intensity per channel) of the area indicated by the white dotted line in the zoomed merged image.

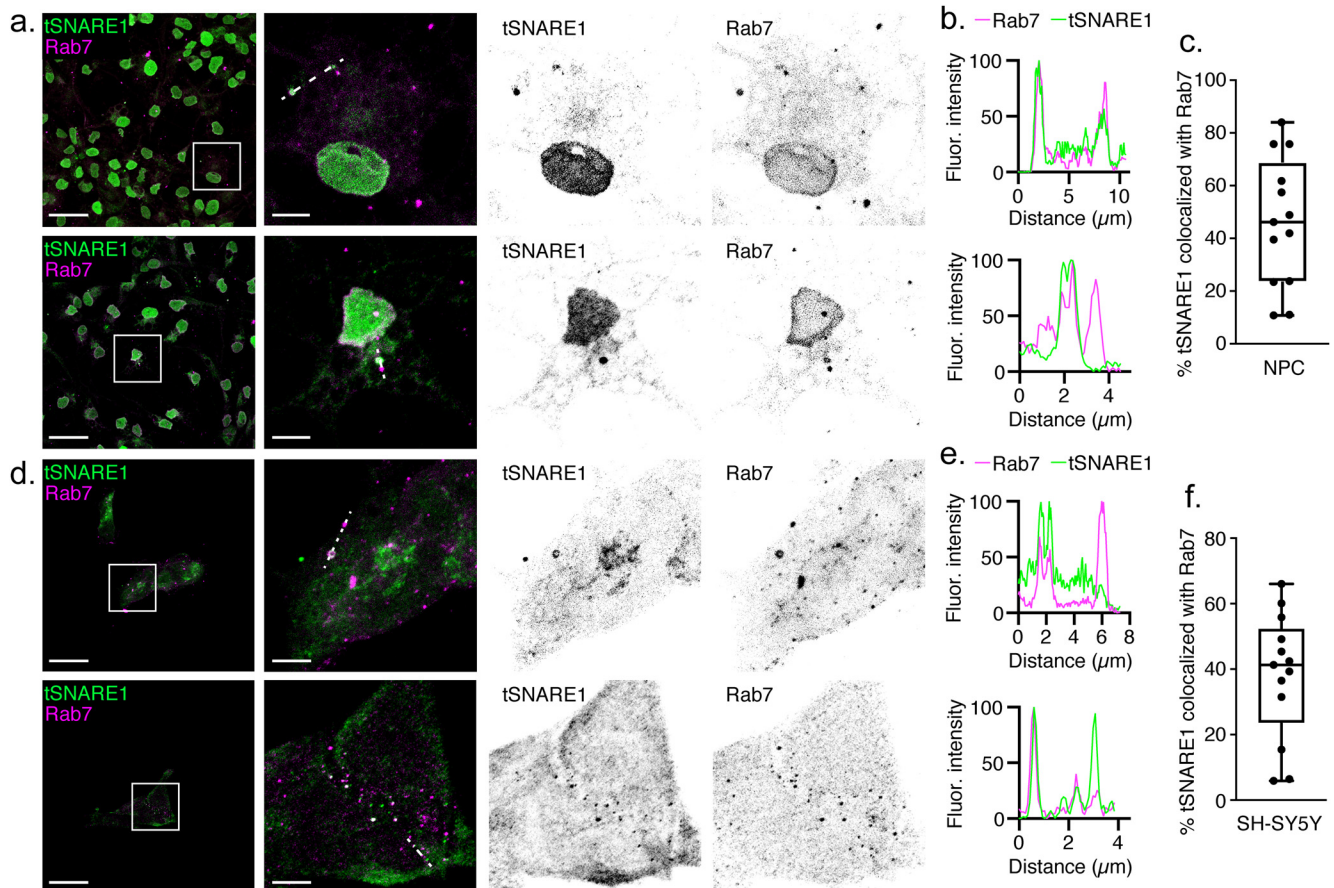


Figure 7. Endogenous tSNARE1 localizes to Rab7⁺ compartments in primary human neural progenitors and neuroblastoma cells. *a*, Maximum intensity projections of primary human NPCs immunostained for tSNARE1 (green) and Rab7 (magenta). *b*, Average 3 pixel-wide line scans of the fluorescence intensity of tSNARE1 and Rab7 in a single z plane (normalized to the minimum and maximum fluorescence intensity per channel) of the area denoted by the white dotted line shown in the zoomed merged image of each row in *a*. *c*, The percent of the volume of endogenous tSNARE1 that was colocalized with Rab7 in NPCs ($n = 13$ cells). *d*, Maximum intensity projections of human SH-SY5Y neuroblastoma cells immunostained for tSNARE1 (green) and Rab7 (magenta). *e*, Average 3 pixel-wide line scans of the fluorescence intensity of tSNARE1 and Rab7 in a single z plane (normalized to the minimum and maximum fluorescence intensity per channel) of the area denoted by the white dotted line shown in the zoomed merged image of each row in *d*. *f*, The percent of the volume of endogenous tSNARE1 that colocalized with Rab7 in SH-SY5Y neuroblastoma cells ($n = 13$ cells). For each row in *a* and *c*, there is a zoomed-out image (left) with a zoomed-in ROI (right). Beside this are inverted contrast images of each channel from the merged images. Scale bars: left column, 25 μm ; zoomed images, 5 μm . Colocalization data are reported in a box-and-whiskers plot, with the minimum and maximum values as whiskers and the median and the 25th and 75th percentile as the box.

revealed that tSNARE1 localized to both Tau⁺ axons and MAP2⁺ dendrites (Fig. 9*b,c*). These data suggested that tSNARE1 localizes to both axonal and dendritic processes in human neurons.

Because rat cortical neurons mature and form synapses *in vitro* more robustly than mouse or human neurons, we used rat neurons to interrogate tSNARE1 localization in mature neurons. Similar to the previous data, GFP-tSNARE1c was most abundant in the soma in rat neurons at 15 DIV, but there was a population of GFP-tSNARE1c that localized to the processes visualized with CAAX-tagRFP, which labels the plasma membrane (Fig. 9*d*). Because schizophrenia is typified by a decreased density of dendritic spines (Garey et al., 1998; Glantz and Lewis, 2000; Glausier and Lewis, 2013), and lysosomes traffic to dendritic spines (Goo et al., 2017), we hypothesized that tSNARE1 may localize to the postsynapse. Indeed, we found a striking colocalization of GFP-tSNARE1c with an intrabody marker for the postsynaptic protein PSD95 (Rimbault et al., 2021) in rat cortical neurons at 22 DIV (Fig. 9*e–g*). These data demonstrate that tSNARE1 colocalizes with PSD95 at dendritic shafts and dendritic spines and suggests that tSNARE1 likely functions at the postsynapse.

Discussion

Although many genetic loci are implicated in schizophrenia, without understanding the function of the implicated gene products, the etiology of schizophrenia will remain unclear. *TSNARE1* is a high-confidence gene candidate for schizophrenia risk, but its biological function in the brain was previously unknown. We identified the three most abundant mRNA products of *TSNARE1*, the sequence information from which gave clues as to their likely biological function. Collectively, the *TSNARE1* mRNAs encoded two potential functional domains: a predicted syntaxin-like Qa SNARE domain, present in all three isoforms, and an Myb-like domain that is present in two of the three isoforms. Whereas the data we presented do not eliminate a possible role for the Myb-like domain in schizophrenia pathogenesis associated with *TSNARE1*, the weight of data presented here point most strongly to a role for tSNARE1 as a regulator of membrane trafficking in the endolysosomal system. This function is most likely key to both its normal activity within neurons as well as its dysfunction, which is associated with schizophrenia.

What are the features related to human *TSNARE1* that suggest that its biological function is linked to endosomal trafficking? First, all isoforms contained the Qa SNARE domain while

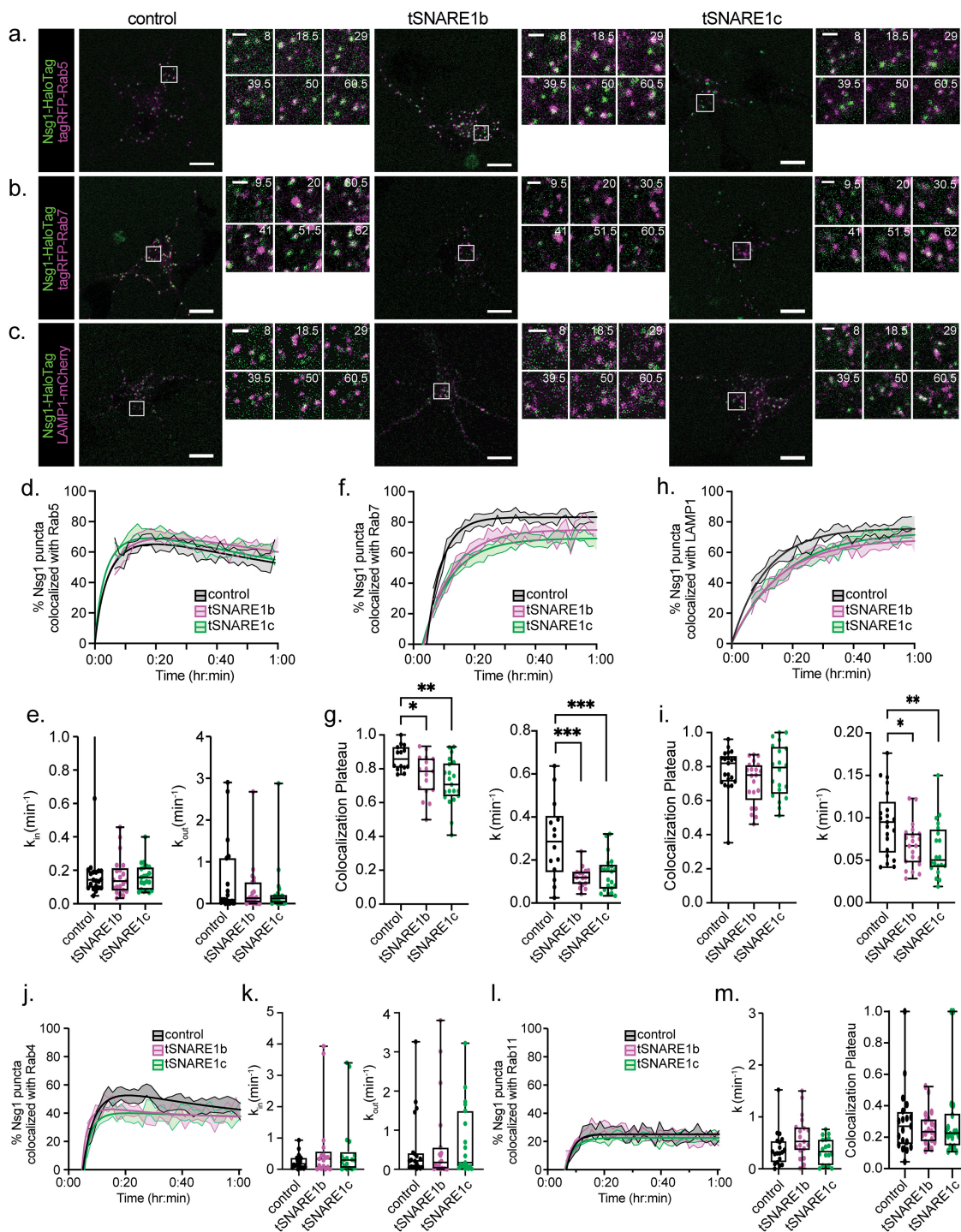
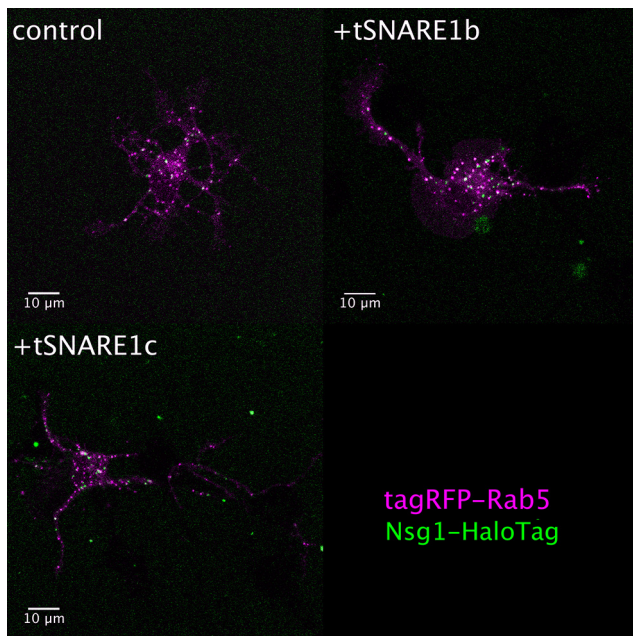
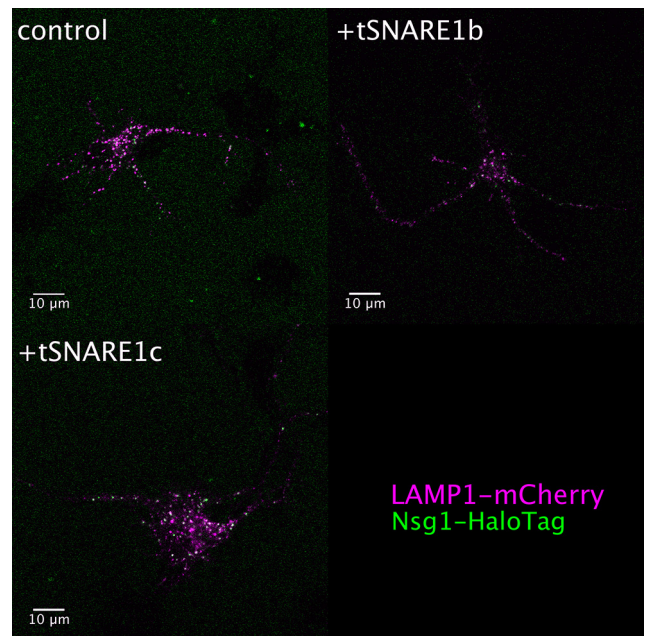


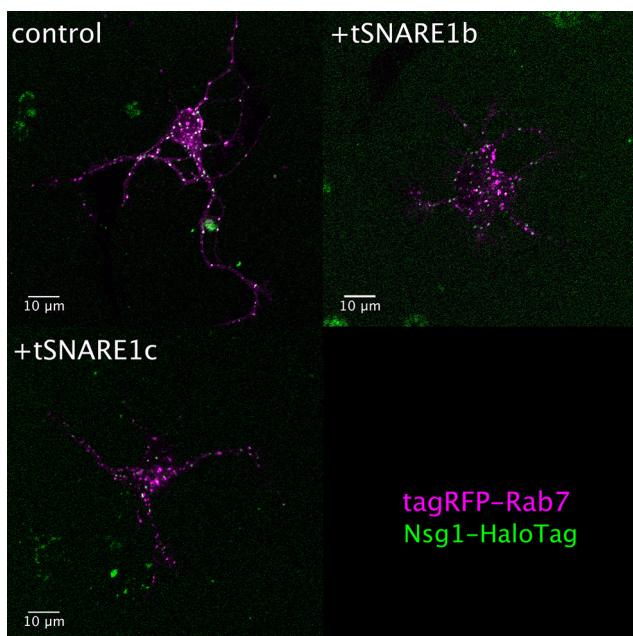
Figure 8. Overexpression of tSNARE1 delays trafficking of Nsg1 into late endosomal and lysosomal compartments. **a–c**, A representative single frame from each movie of a mouse cortical neuron at 2 DIV-expressing Nsg1-HaloTag (AlexaFluor-660 ligand) and (**a**) tagRFP-Rab5, (**b**) tagRFP-Rab7, or (**c**) LAMP1-mCherry, with or without the GFP-tSNARE1 isoforms listed. Scale bars: large, 10 μ m; zoom montage, 2 μ m. Time is in minutes. **d**, The percentage of Nsg1-HaloTag puncta colocalized with tagRFP-Rab5 over time. $n = 22$ (control), $n = 21$ (tSNARE1b), $n = 21$ (tSNARE1c). **e**, Nsg1-HaloTag entry into (k_{in}) or exit out of (k_{out}) tagRFP-Rab5⁺ compartments. k_{in} $p = 0.3710$ (tSNARE1b), $p = 0.3701$ (tSNARE1c); k_{out} $p = 0.4922$ (tSNARE1b), $p = 0.3634$ (tSNARE1c). **f**, The percentage of Nsg1-HaloTag puncta colocalized with tagRFP-Rab7 over time. $n = 14$ (control), $n = 17$ (tSNARE1b), $n = 21$ (tSNARE1c). **g**, The colocalization plateau and rate constant for Nsg1-HaloTag entry into tagRFP-Rab7⁺ compartments. Plateau $p = 0.0291$ (tSNARE1b), $p = 0.0016$ (tSNARE1c); k $p = 0.0002$ (tSNARE1b), $p = 0.0004$ (tSNARE1c). **h**, The percentage of Nsg1-HaloTag puncta colocalized with LAMP1-mCherry over time. $n = 21$ (control), $n = 21$ (tSNARE1b), $n = 20$ (tSNARE1c). **i**, The colocalization plateau and the rate constant for Nsg1-HaloTag entry into LAMP1-mCherry⁺ compartments. Plateau $p = 0.1940$ (tSNARE1b), $p = 0.9960$ (tSNARE1c); k $p = 0.0192$ (tSNARE1b), $p = 0.0051$ (tSNARE1c). **j**, The percentage of Nsg1-HaloTag puncta colocalized with tagRFP-Rab4 over time. $n = 20$ (control), $n = 17$ (tSNARE1b), $n = 18$ (tSNARE1c). **k**, Nsg1-HaloTag entry into (k_{in}) or exit out of (k_{out}) tagRFP-Rab4⁺ compartments. k_{in} $p = 0.2428$ (tSNARE1b) and $p = 0.3504$ (tSNARE1c), k_{out} $p = 0.8819$ (tSNARE1b) and $p = 0.7632$ (tSNARE1c). **l**, The percentage of Nsg1-HaloTag puncta colocalized with tagRFP-Rab11 over time. $n = 19$ (control), $n = 19$ (tSNARE1b), $n = 18$ (tSNARE1c). **m**, The colocalization plateau and rate constant for Nsg1-HaloTag entry into tagRFP-Rab11⁺ compartments. k $p = 0.0871$ (tSNARE1b), $p = 0.9215$ (tSNARE1c); plateau $p = 0.7619$ (tSNARE1b), $p = 0.9890$ (tSNARE1c). Data are reported by the curve fit (dark line, see Materials and Methods) of the mean percentage \pm SEM (shaded area) at each time point. For the quantification of rates and colocalization plateaus, data are reported in a box-and-whiskers plot, with the minimum and maximum values as whiskers and the median and the 25th and 75th percentile as the box. * $p < 0.05$; ** $p < 0.005$; *** $p < 0.0005$; one-way ANOVA. n refers to the number of cells examined.



Movie 1. Nsg1-HaloTag colocalization with tagRFP-Rab5 over time. [View online]



Movie 3. Nsg1-HaloTag colocalization with LAMP1-mCherry over time. [View online]



Movie 2. Nsg1-HaloTag colocalization with tagRFP-Rab7 over time. [View online]

only a subset of these included the Myb domain, and it is the collective overexpression of these isoforms that is associated with schizophrenia in humans. Second, just as overexpression of tSNARE1 is associated with schizophrenia, we found that overexpression of either of the two most common forms of tSNARE1 in mouse neurons altered endosomal trafficking. Third, recombinant forms of tSNARE1 inhibited Stx12 incorporation into early endosomal SNARE complexes, supporting a possible role as an i-SNARE in early endosome maturation into late endosomes. Finally, other endosomal regulators have been linked to schizophrenia pathogenesis. For example, *SNAP91* is another high-confidence candidate gene for schizophrenia and appears to

genetically interact with *TSNARE1* (Wang et al., 2018; Schrode et al., 2019). Further, the copy number variant at chromosome 22q11.2, which is strongly associated with schizophrenia, includes the gene *SNAP29*, which has been shown to have roles in endocytosis and autophagy (Mastrodonato et al., 2018; Forsyth et al., 2020). Even beyond schizophrenia, endosomal machinery has been linked to other neuropsychiatric and neurodevelopmental disorders, such as in Christianson syndrome with *NHE6* that is involved in acidification of endosomes (Ilie et al., 2020). Together, these observations provide a compelling case for the role of tSNARE1 in schizophrenia being at the level of endosomal trafficking, likely in the trafficking or maturation of early endosomes to late endosomes.

Why then does the *TSNARE1* gene contain exons encoding an Myb-like domain? The Myb-like domain has several nuclear localization signals associated with the DNA-binding activity of this domain. While we cannot exclude a function for tSNARE1 in the nucleus, one likely explanation is that the *TSNARE1* gene arose during vertebrate evolution as a product of a Harbinger transposition (Sinzelle et al., 2008; Smith et al., 2012). Since the Myb domain descended from the DNA-binding protein of the Harbinger transposon that is required for the transposition event itself, its presence may simply be a relic of this transposition. Alternatively, the nuclear localization may act to regulate the partitioning of tSNARE1 in and out of the nucleus to control the level of tSNARE1 in the cytoplasm.

A majority (~93%-97%) of tSNARE1 in the brain (two of the three isoforms) lacked a TM domain or a predicted lipid attachment site, which is critical for membrane fusion facilitated by Qa-family SNARE proteins (Spessott et al., 2017). This is an important difference, as Qa SNAREs lacking a TM domain would likely inhibit, rather than promote, membrane fusion. Therefore, tSNARE1 has the properties previously predicted by Rothman and colleagues of an i-SNARE (Varlamov et al., 2004). i-SNAREs were proposed as a mechanism to modulate membrane trafficking events through the formation of fusion-incompetent complexes. These fusion-incompetent complexes would thereby act as competitive inhibitors to the formation of canonical fusion-

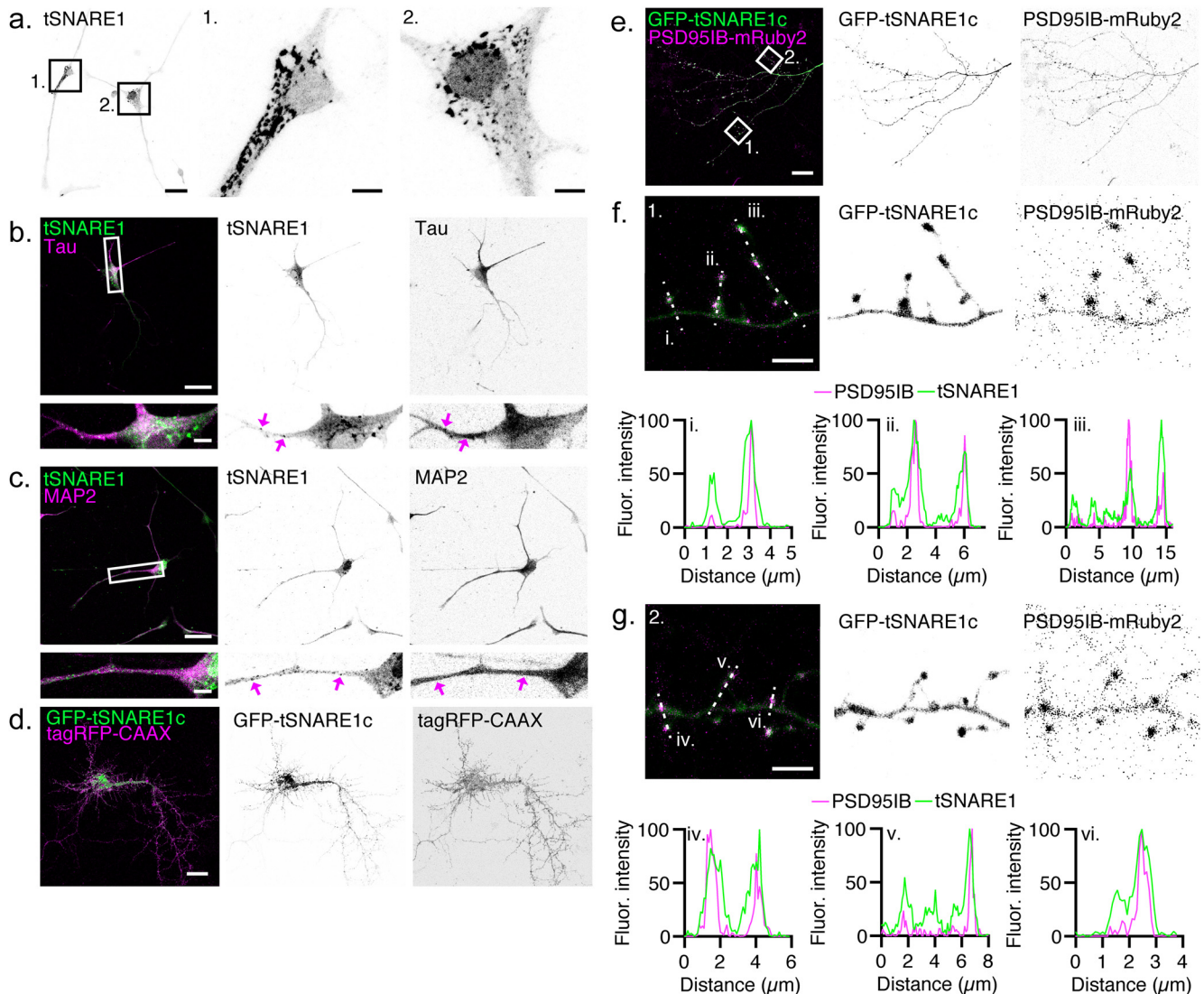


Figure 9. tSNARE1 localizes to axons, dendrites, and the postsynapse. **a**, A reverse-contrast maximum intensity projection of human neurons differentiated from primary human NPCs immunostained for tSNARE1. Right, Enlarged black boxes represent ROIs. Scale bars: left, 25 μm ; zoomed images, 5 μm . **b**, **c**, Maximum intensity projections of NPC-derived human neurons depicting endogenous tSNARE1 (green) and either (**b**) Tau (magenta), localization seen in $n = 11$ of 12 cells or (**c**) MAP2 (magenta), localization seen in $n = 12$ of 13 cells. Enlarged white rectangle represents ROI. Right, Reverse-contrast images of each channel. Magenta arrows point to areas positive for both tSNARE1 and the respective marker. Scale bars: left, 25 μm ; zoomed images, 5 μm . **d**, Maximum intensity projection of GFP-tSNARE1c (green) and tagRFP-CAAX (magenta) in a 15 DIV E18 rat cortical neuron. Left, Merged image. Right, Separated reverse-contrast images of each channel. Scale bar, 25 μm . **e**, Maximum intensity projection of GFP-tSNARE1c (green) and PSD95IB-mRuby2 (magenta) in a dendritic arbor of a 22 DIV E18 rat cortical neuron. Right, Reverse-contrast images of each channel. Scale bar, 25 μm . We observed this localization in $n = 8$ of 8 cells. **f**, **g**, Zoomed maximum intensity projection of the ROIs denoted in **e**. For each, 3 pixel-wide average line scans of a single z plane are displayed for each region indicated by the dashed white lines in the merged image. Right, Reverse-contrast images of each channel. Scale bar, 5 μm .

competent SNARE complexes. In the case of tSNARE1, the most likely target of this inhibition is Stx12, which is thought to function in endosomal trafficking. Our biochemical demonstration that tSNARE1c can indeed form ternary SNARE complexes with the same three endosomal SNAREs as Stx12 and that tSNARE1 competes with Stx12 for incorporation into this SNARE complex fits with this possibility. While i-SNAREs have been predicted and demonstrated *in vitro*, we believe this is likely the first example of an i-SNARE implicated in human disease. Therefore, the inhibitory function of tSNARE1 is likely central to both its normal mechanism of action as well as its role in schizophrenia when overexpressed.

Previous reports suggested tSNARE1 is likely to function in synaptic vesicle exocytosis (Sleiman et al., 2013; Gu et al., 2015; Fromer et al., 2016; Schrode et al., 2019). However, this

statement is most likely related to confusion over classification of tSNARE1 as a “target” SNARE protein based on it being related to the syntaxin family of Q-SNARE proteins, whereas its specific role in the cell was completely uninvestigated. The syntaxin family member Stx1 does indeed have a well-documented role in synaptic vesicle exocytosis, but the protein sequence of tSNARE1 is most closely associated with Stx12, which is thought to be involved in endosome: endosome fusion necessary for maturation of early endosomes into late endosomes (Wandinger-Ness and Zerial, 2014). Therefore, tSNARE1 is highly unlikely to function in synaptic release directly. Indeed, we showed that tSNARE1 is localized to the endolysosomal system rather than to the plasma membrane where Stx1 is found (Bennett et al., 1992). Further, these previous studies use, to our knowledge, a human isoform of tSNARE1, which contains a TM

domain (tSNARE1a), which we find only represents 3%–7% of tSNARE1 in human brain.

We found that the non-TM forms of tSNARE1, tSNARE1b, and tSNARE1c most frequently populated and delayed Nsg1 trafficking into Rab7⁺ late endosomal compartments. However, tSNARE1 did not cause a significant delay trafficking out of the early endosome. One possible explanation for this result could be that there is increased retrieval of Nsg1 from the late endosome to the early endosome. However, if this were true, we would expect the colocalization of Nsg1 with Rab5⁺ early endosomes to increase over time or reach a steady state, which is not what we observed. An alternative hypothesis is that tSNARE1 increases the trafficking of Nsg1 to a different endosomal compartment. Yet, we found that tSNARE1 had no effect on Nsg1 trafficking into the recycling endosomes marked by either Rab4 or Rab11. However, the possibility remains that tSNARE1 may regulate traffic to an endosomal compartment not marked by Rab4, Rab5, Rab7, Rab11, or LAMP1, or our assay may not be sufficiently sensitive to detect small changes in rates of endosomal flux through the early and recycling endosomes in the relatively short time frames examined. Although the precise step in the delay of Nsg1 to the late endosome and the lysosome is unknown, the fact that we observed this delay suggests that tSNARE1 overexpression has clear physiological consequences during transport to the late endosome/lysosome.

In this paper, we demonstrated that *TSNARE1* is a risk factor for schizophrenia, and its gene products are critical regulators of endosomal trafficking. Yet, how tSNARE1 dysfunction contributes to schizophrenia pathogenesis is unknown. Our results suggest that tSNARE1 is enriched in the soma but also localizes to both axons and dendrites. This finding brings up an exciting possibility that tSNARE1 may be poised to function at the synapse. For example, tSNARE1 may alter the availability of machinery needed for synaptic release at the presynapse or regulate receptor availability or protein homeostasis at the postsynapse. Schizophrenia is particularly characterized by a decrease in the density of dendritic spines (Garey et al., 1998; Glantz and Lewis, 2000; Glausier and Lewis, 2013), and lysosomes traffic into the dendritic shaft and dendritic spines presumably to regulate synaptic remodeling or pruning through local degradation (Goo et al., 2017). These points led us to hypothesize that tSNARE1 may also play a role at the postsynapse. Indeed, we observed that tSNARE1 localized to the dendritic shaft and dendritic spines in mature rat cortical neurons and altered the trafficking of the dendritic protein Nsg1 in developing mouse cortical neurons. These observations support a role for tSNARE1 at the synapse, particularly at the postsynapse. The fact that overexpression of tSNARE1 is linked to schizophrenia suggests that the membrane trafficking events that tSNARE1 regulates require precise levels of tSNARE1. For example, as an i-SNARE, tSNARE1 overexpression may negatively regulate a trafficking event that affects lysosomal turnover in the dendrite during synaptic remodeling. Determining the specific trafficking events that tSNARE1 regulates and how tSNARE1 functions at the synapse is critical toward understanding how its dysfunction is associated with schizophrenia. These observations may reveal common pathways disrupted in schizophrenia and possible targets for drug design and clinical intervention.

References

Antonin W, Fasshauer D, Becker S, Jahn R, Schneider TR (2002) Crystal structure of the endosomal SNARE complex reveals common structural principles of all SNAREs. *Nat Struct Biol* 9:107–111.

- Barford K, Yap CC, Dwyer ND, Winckler B (2017) The related neuronal endosomal proteins NEEP21 (Nsg1) and P19 (Nsg2) have divergent expression profiles in vivo. *J Comp Neurol* 525:1861–1878.
- Bennett MK, Calakos N, Scheller RH (1992) Syntaxin: a synaptic protein implicated in docking of synaptic vesicles at presynaptic active zones. *Science* 257:255–259.
- Bradford MM (1976) A rapid and sensitive method for the quantitation of microgram quantities of protein utilizing the principle of protein-dye binding. *Anal Biochem* 72:248–254.
- Clary DO, Griff IC, Rothman JE (1990) SNAPs, a family of NSF attachment proteins involved in intracellular membrane fusion in animals and yeast. *Cell* 61:709–721.
- Darmanis S, Sloan SA, Zhang Y, Enge M, Caneda C, Shuer LM, Hayden Gephart MG, Barres BA, Quake SR (2015) A survey of human brain transcriptome diversity at the single cell level. *Proc Natl Acad Sci USA* 112:7285–7290.
- de la Torre-Ubieta L, Stein JL, Won H, Opland CK, Liang D, Lu D, Geschwind DH (2018) The dynamic landscape of open chromatin during human cortical neurogenesis. *Cell* 172:289–304.e18.
- Diering GH, Gustina AS, Haganir RL (2014) PKA-GluA1 coupling via AKAP5 controls AMPA receptor phosphorylation and cell-surface targeting during bidirectional homeostatic plasticity. *Neuron* 84:790–805.
- Fasshauer D, Sutton RB, Brunger AT, Jahn R (1998) Conserved structural features of the synaptic fusion complex: SNARE proteins reclassified as Q- and R-SNAREs. *Proc Natl Acad Sci USA* 95:15781–15786.
- Forsyth JK, Nachun D, Gandal MJ, Geschwind DH, Anderson AE, Coppola G, Bearden CE (2020) Synaptic and gene regulatory mechanisms in schizophrenia, autism, and 22q11.2 copy number variant-mediated risk for neuropsychiatric disorders. *Biol Psychiatry* 87:150–163.
- Fromer M, Roussos P, Sieberts SK, Johnson JS, Kavanagh DH, Perumal TM, Ruderfer DM, Oh EC, Topol A, Shah HR, Klei LL, Kramer R, Pinto D, Gümüş ZH, Cicek AE, Dang KK, Browne A, Lu C, Xie L, Readhead B, et al. (2016) Gene expression elucidates functional impact of polygenic risk for schizophrenia. *Nat Neurosci* 19:1442–1453.
- Gandal MJ, Zhang P, Hadjimichael E, Walker RL, Chen C, Liu S, Won H, van Bakel H, Varghese M, Wang Y, Shieh AW, Haney J, Parhami S, Belmont J, Kim M, Moran Losada P, Khan Z, Mleczko J, Xia Y, Dai R, et al. (2018) Transcriptome-wide isoform-level dysregulation in ASD, schizophrenia, and bipolar disorder. *Science* 362:eaat8127.
- Garey LJ, Ong WY, Patel TS, Kanani M, Davis A, Mortimer AM, Barnes TR, Hirsch SR (1998) Reduced dendritic spine density on cerebral cortical pyramidal neurons in schizophrenia. *J Neurol Neurosurg Psychiatry* 65:446–453.
- Glantz LA, Lewis DA (2000) Decreased dendritic spine density on prefrontal cortical pyramidal neurons in schizophrenia. *Arch Gen Psychiatry* 57:65–73.
- Glausier JR, Lewis DA (2013) Dendritic spine pathology in schizophrenia. *Neuroscience* 251:90–107.
- Goo MS, Sancho L, Slepak N, Boassa D, Deerinck TJ, Ellisman MH, Bloodgood BL, Patrick GN (2017) Activity-dependent trafficking of lysosomes in dendrites and dendritic spines. *J Cell Biol* 216:2499–2513.
- Gu LZ, Jiang T, Cheng ZH, Zhang YC, Ou MM, Chen MC, Ling WM (2015) TSNARE1 polymorphisms are associated with schizophrenia susceptibility in Han Chinese. *J Neural Transm (Vienna)* 122:929–932.
- Hanson PI, Roth R, Morisaki H, Jahn R, Heuser JE (1997) Structure and conformational changes in NSF and its membrane receptor complexes visualized by quick-freeze/deep-etch electron microscopy. *Cell* 90:523–535.
- Hofmann MW, Peplowska K, Rohde J, Poschner BC, Ungermann C, Langosch D (2006) Self-interaction of a SNARE transmembrane domain promotes the hemifusion-to-fusion transition. *J Mol Biol* 364:1048–1060.
- Ilie A, Boucher A, Park J, Berghuis AM, McKinney RA, Orlowski J (2020) Assorted dysfunctions of endosomal alkali cation/proton exchanger SLC9A6 variants linked to Christianson syndrome. *J Biol Chem* 295:7075–7095.
- Janssen J, Alemán-Gómez Y, Schnack H, Balaban E, Pina-Camacho L, Alfaro-Almagro F, Castro-Fornieles J, Otero S, Baeza I, Moreno D, Bargalló N, Parellada M, Arango C, Descó M (2014) Cortical morphology of adolescents with bipolar disorder and with schizophrenia. *Schizophr Res* 158:91–99.
- Kapitonov VV, Jurka J (2004) Harbinger transposons and an ancient HARBII gene derived from a transposase. *DNA Cell Biol* 23:311–324.

- Lake BB, Ai R, Kaeser GE, Salathia NS, Yung YC, Liu R, Wildberg A, Gao D, Fung HL, Chen S, Vijayaraghavan R, Wong J, Chen A, Sheng X, Kaper F, Shen R, Ronaghi M, Fan JB, Wang W, Chun J, et al. (2016) Neuronal subtypes and diversity revealed by single-nucleus RNA sequencing of the human brain. *Science* 352:1586–1590.
- Larson BT, Sochacki KA, Kindem JM, Taraska JW (2014) Systematic spatial mapping of proteins at exocytic and endocytic structures. *Mol Biol Cell* 25:2084–2093.
- Lin RC, Scheller RH (1997) Structural organization of the synaptic exocytosis core complex. *Neuron* 19:1087–1094.
- Mah W, Won H (2020) The three-dimensional landscape of the genome in human brain tissue unveils regulatory mechanisms leading to schizophrenia risk. *Schizophr Res* 217:17–25.
- Mastrodonato V, Morelli E, Vaccari T (2018) How to use a multipurpose SNARE: the emerging role of Snap29 in cellular health. *Cell Stress* 2:72–81.
- Miller JA, Ding SL, Sunkin SM, Smith KA, Ng L, Szafer A, Ebbert A, Riley ZL, Royall JJ, Aiona K, Arnold JM, Bennet C, Bertagnolli D, Brouner K, Butler S, Caldejon S, Carey A, Cuhaciyan C, Dalley RA, Dee N, et al. (2014) Transcriptional landscape of the prenatal human brain. *Nature* 508:199–206.
- Nichols BJ, Ungermann C, Pelham HR, Wickner WT, Haas A (1997) Homotypic vacuolar fusion mediated by t- and v-SNAREs. *Nature* 387:199–202.
- Pardiñas AF, Holmans P, Pocklington AJ, Escott-Price V, Ripke S, Carrera N, Legge SE, Bishop S, Cameron D, Hamshere ML, Han J, Hubbard L, Lynham A, Mantripragada K, Rees E, MacCabe JH, McCarroll SA, Baune BT, Breen G, Byrne EM, et al. (2018) Common schizophrenia alleles are enriched in mutation-intolerant genes and in regions under strong background selection. *Nat Genet* 50:381–389.
- Parlati F, Varlamov O, Paz K, McNew JA, Hurtado D, Söllner TH, Rothman JE (2002) Distinct SNARE complexes mediating membrane fusion in Golgi transport based on combinatorial specificity. *Proc Natl Acad Sci USA* 99:5424–5429.
- Pollard KS, Hubisz MJ, Rosenbloom KR, Siepel A (2010) Detection of non-neutral substitution rates on mammalian phylogenies. *Genome Res* 20:110–121.
- Rimbault C, Breillat C, Compans B (2021) Engineering paralog-specific PSD-95 synthetic binders as potent and minimally invasive imaging probes. *bioRxiv* 2021.04.07.438431.
- Rimol LM, Hartberg CB, Nesvåg R, Fennema-Notestine C, Hagler DJ, Pung CJ, Jennings RG, Haukvik UK, Lange E, Nakstad PH, Melle I, Andreassen OA, Dale AM, Agartz I (2010) Cortical thickness and subcortical volumes in schizophrenia and bipolar disorder. *Biol Psychiatry* 68:41–50.
- Rossi G, Salminen A, Rice LM, Brunger AT, Brennwald P (1997) Analysis of a yeast SNARE complex reveals remarkable similarity to the neuronal SNARE complex and a novel function for the C terminus of the SNAP-25 homolog, Sec9. *J Biol Chem* 272:16610–16617.
- Rothman JE (1994) Mechanisms of intracellular protein transport. *Nature* 372:55–63.
- Schindelin J, Arganda-Carreras I, Frise E, Kaynig V, Longair M, Pietzsch T, Preibisch S, Rueden C, Saalfeld S, Schmid B, Tinevez JY, White DJ, Hartenstein V, Eliceiri K, Tomancak P, Cardona A (2012) Fiji: an open-source platform for biological-image analysis. *Nat Methods* 9:676–682.
- Schindelin J, Rueden CT, Hiner MC, Eliceiri KW (2015) The ImageJ ecosystem: an open platform for biomedical image analysis. *Mol Reprod Dev* 82:518–529.
- Schizophrenia Working Group of the Psychiatric Genomics Consortium (2014) Biological insights from 108 schizophrenia-associated genetic loci. *Nature* 511:421–427.
- Schneider CA, Rasband WS, Eliceiri KW (2012) NIH Image to ImageJ: 25 years of image analysis. *Nat Methods* 9:671–675.
- Schrode N, Ho SM, Yamamuro K, Dobbyn A, Huckins L, Matos MR, Cheng E, Deans PJ, Flaherty E, Barretto N, Topol A, Alganem K, Abadali S, Gregory J, Hoelzli E, Phatnani H, Singh V, Girish D, Aronow B, McCullumsmith R, et al. (2019) Synergistic effects of common schizophrenia risk variants. *Nat Genet* 51:1475–1485.
- Sey NY, Hu B, Mah W, Fauni H, McAfee JC, Rajarajan P, Brennand KJ, Akbarian S, Won H (2020) A computational tool (H-MAGMA) for improved prediction of brain-disorder risk genes by incorporating brain chromatin interaction profiles. *Nat Neurosci* 23:583–593.
- Sinzelle L, Kapitonov VV, Grzela DP, Jursch T, Jurka J, Izsvák Z, Ivics Z (2008) Transposition of a reconstructed Harbinger element in human cells and functional homology with two transposon-derived cellular genes. *Proc Natl Acad Sci USA* 105:4715–4720.
- Skene NG, Bryois J, Bakken TE, Breen G, Crowley JJ, Gaspar HA, Giusti-Rodriguez P, Hodge RD, Miller JA, Muñoz-Manchado AB, O'Donovan MC, Owen MJ, Pardiñas AF, Ryge J, Walters JT, Linnarsson S, Lein ES, Sullivan PF, Hjerling-Leffler J; Major Depressive Disorder Working Group of the Psychiatric Genomics Consortium (2018) Genetic identification of brain cell types underlying schizophrenia. *Nat Genet* 50:825–833.
- Sleiman P, Wang D, Glessner J, Hadley D, Gur RE, Cohen N, Li Q, Hakonarson H; Janssen-CHOP Neuropsychiatric Genomics Working Group (2013) GWAS meta analysis identifies TSNARE1 as a novel Schizophrenia/Bipolar susceptibility locus. *Sci Rep* 3:3075.
- Smith JJ, Sumiyama K, Amemiya CT (2012) A living fossil in the genome of a living fossil: harbinger transposons in the coelacanth genome. *Mol Biol Evol* 29:985–993.
- Söllner T, Whiteheart SW, Brunner M, Erdjument-Bromage H, Geromanos S, Tempst P, Rothman JE (1993) SNAP receptors implicated in vesicle targeting and fusion. *Nature* 362:318–324.
- Spessott WA, Sanmillan ML, McCormick ME, Kulkarni VV, Giraudo CG (2017) SM protein Munc18-2 facilitates transition of Syntaxin 11-mediated lipid mixing to complete fusion for T-lymphocyte cytotoxicity. *Proc Natl Acad Sci USA* 114:E2176–E2185.
- Steiner P, Sarria JC, Glauser L, Magnin S, Catsicas S, Hirling H (2002) Modulation of receptor cycling by neuron-enriched endosomal protein of 21 kD. *J Cell Biol* 157:1197–1209.
- van de Leemput J, Boles NC, Kiehl TR, Corneo B, Lederman P, Menon V, Lee C, Martinez RA, Levi BP, Thompson CL, Yao S, Kaykas A, Temple S, Fasano CA (2014) CORTECON: a temporal transcriptome analysis of in vitro human cerebral cortex development from human embryonic stem cells. *Neuron* 83:51–68.
- Varlamov O, Volchuk A, Rahimian V, Doege CA, Paumet F, Eng WS, Arango N, Parlati F, Ravazzola M, Orci L, Söllner TH, Rothman JE (2004) i-SNAREs: inhibitory SNAREs that fine-tune the specificity of membrane fusion. *J Cell Biol* 164:79–88.
- Wandinger-Ness A, Zerial M (2014) Rab proteins and the compartmentalization of the endosomal system. *Cold Spring Harb Perspect Biol* 6:a022616.
- Wang D, Liu S, Warrell J, Won H, Shi X, Navarro FC, Clarke D, Gu M, Emani P, Yang YT, Xu M, Gandal MJ, Lou S, Zhang J, Park JJ, Yan C, Rhie SK, Manakongtreecheep K, Zhou H, Nathan A, et al. (2018) Comprehensive functional genomic resource and integrative model for the human brain. *Science* 362:eaat8464.
- Yap CC, Digilio L, McMahon L, Winckler B (2017) The endosomal neuronal proteins Nsg1/NEEP21 and Nsg2/P19 are itinerant, not resident proteins of dendritic endosomes. *Sci Rep* 7:10481.
- Zwilling D, Cypionka A, Pohl WH, Fasshauer D, Walla PJ, Wahl MC, Jahn R (2007) Early endosomal SNAREs form a structurally conserved SNARE complex and fuse liposomes with multiple topologies. *EMBO J* 26:9–18.